Journal of the Mechanics and Physics of Solids 94 (2016) 127–147

Contents lists available at ScienceDirect

Journal of the Mechanics and Physics of Solids

journal homepage: www.elsevier.com/locate/jmps

A constitutive model of nanocomposite hydrogels with nanoparticle crosslinkers

Qiming Wang *, Zheming Gao

Sonny Astani Department of Civil and Environmental Engineering, University of Southern California, Los Angeles, CA 90089, USA

ARTICLE INFO

Article history:
Received 14 December 2015
Received in revised form
11 April 2016
Accepted 11 April 2016
Available online 16 April 2016

Keywords:
Tough hydrogel
Constitutive model
Network alteration model
Eight-chain model
Chain length distribution

ABSTRACT

Nanocomposite hydrogels with only nanoparticle crosslinkers exhibit extraordinarily higher stretchability and toughness than the conventional organically crosslinked hydrogels, thus showing great potential in the applications of artificial muscles and cartilages. Despite their potential, the microscopic mechanics details underlying their mechanical performance have remained largely elusive. Here, we develop a constitutive model of the nanoparticle hydrogels to elucidate the microscopic mechanics behaviors, including the microarchitecture and evolution of the nanoparticle crosslinked polymer chains during the mechanical deformation. The constitutive model enables us to understand the Mullins effect of the nanocomposite hydrogels, and the effects of nanoparticle concentrations and sizes on their cyclic stress–strain behaviors. The theory is quantitatively validated by the tensile tests on a nanocomposite hydrogel with nanosilica crosslinkers. The theory can also be extended to explain the mechanical behaviors of existing hydrogels with nanoclay crosslinkers, and the necking instability of the composite hydrogels with both nanoparticle crosslinkers and organic crosslinkers. We expect that this constitutive model can be further exploited to reveal mechanics behaviors of novel particle-polymer chain interactions, and to design unprecedented hydrogels with both high stretchability and toughness.

1. Introduction

Biocompatible hydrogels with strong sensitivity to external stimuli (e.g., temperature, light and electromagnetic fields) have shown great promise for applications in artificial organs, biological scaffolds and human-centered robotics/actuators (Haraguchi, 2011b; Kamata et al., 2014; Keplinger et al., 2013; Sun et al., 2012; Wang et al., 2010; Zhao, 2014). However, traditional organically crosslinked hydrogels, made of polymer monomers, covalent crosslinkers and water (Fig. 1a), usually suffer from significant limitations in mechanical properties, such as limited stretchability and low fracture toughness. In order to enhance the mechanical properties of the hydrogels, a number of strategies have been proposed recent years to design hydrogels with novel crosslinking agents and tailored molecular architectures (Zhao, 2014). For example, double-network hydrogels have been designed with one network with long polymer chains and the other with shorter polymer chains. Under mechanical loading, the shorter polymer chains are first fractured to partially dissipate the elastic energy, while the hydrogel is still intact due to the backing of the long polymer chains (Gong et al., 2003; Long et al., 2014; Na et al.,

* Corresponding author.
E-mail address: qimingw@usc.edu (Q. Wang).

http://dx.doi.org/10.1016/j.jmps.2016.04.011
0022-5096/

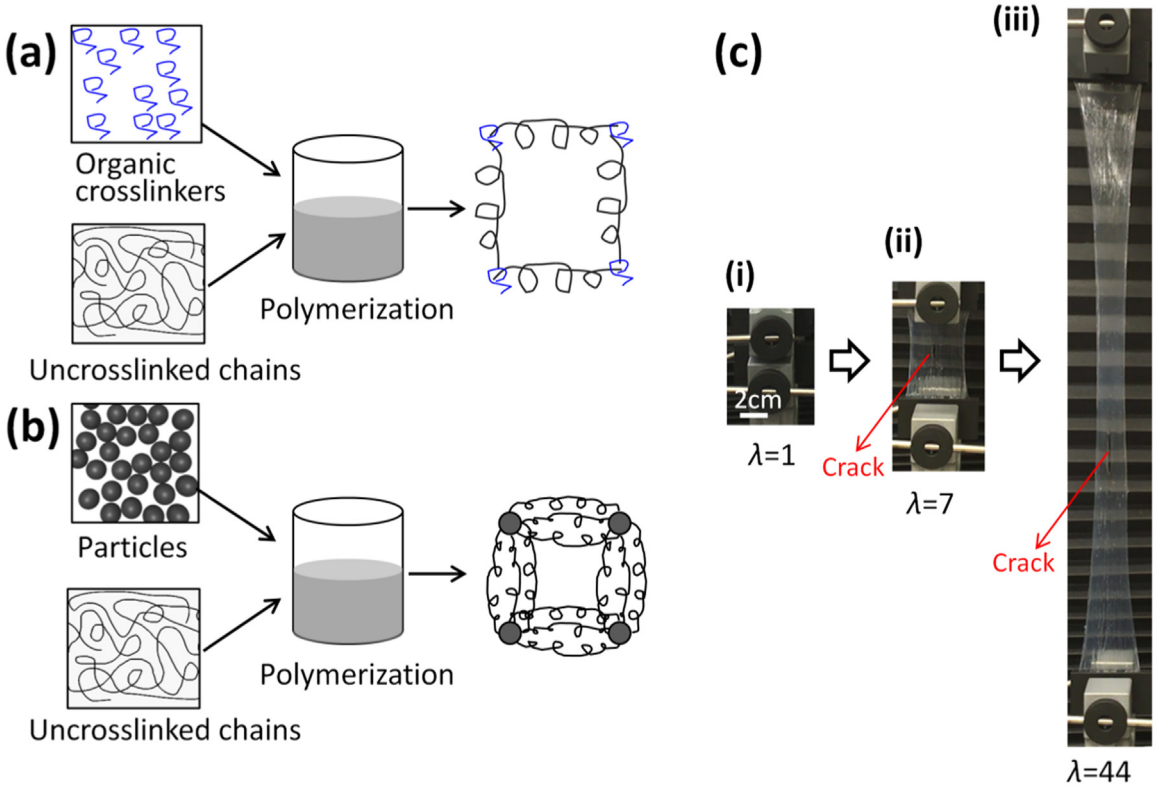

Fig. 1. Fabrication of hydrogels with (a) organic crosslinkers and (b) nanoparticle crosslinkers. (c) Fabricated hydrogels with only nanoparticle crosslinkers can be stretched to 44 times with a small crack within the sample.

2004, 2006; Sun et al., 2012; Tanaka et al., 2005). Following the idea stream, other hydrogels are designed to embed high-functionality crosslinkers that bridge a number of chains with inhomogeneous chain lengths (Fig. 1b) (Haraguchi and Takehisa, 2002; Huang et al., 2007; Wang et al., 2010), so that the portion of short chains may be first detached or fractured under mechanical loading but the long chains can still maintain the elasticity of the hydrogels. In addition, physical crosslinkers have been employed to synthesize hydrogels so that the polymer bonds can be dynamically dissociated to release the mechanical energy, and re-associated repeatedly (An et al., 2010; Hui and Long, 2012; Sun et al., 2012, 2013). Furthermore, hydrogels usually become weak at the swollen state; to address this problem, various crosslinking agents with opposite effects have been embedded into hydrogels to achieve non-swellable hydrogels to maintain good mechanical robustness (Kamata et al., 2014). The aforementioned strategies can be employed separately or integratedly to design hydrogels with high stretchability and toughness (Sun et al., 2012; Sun et al., 2013).

This paper is focused on the hydrogels with polymer networks crosslinked by high-functionality crosslinkers (Flory, 1953). These high-functionality crosslinkers are usually made of inorganic nanoparticles, such as nanoclay, silica, silsesquioxane, titania, graphene oxcide and carbon nanotubes (Carlsson et al., 2010; Haraguchi, 2007, 2011a,b; Haraguchi et al., 2003, 2007, 2002, 2011; Haraguchi and Li, 2006, 2005; Haraguchi and Song, 2007; Haraguchi and Takehisa, 2002; Huang et al., 2007; Ren et al., 2011; Wang et al., 2010).Unlike the organic crosslinkers that usually can only covalently attach several polymer chains around the crosslinkers (e.g., less than 10) due to limited number of connection free-end groups, the nanoparticle crosslinkers with high surface activity are capable of attaching a large number of polymer chains (e.g., more than 100). The attached polymer chains usually have chain lengths over a large range of inhomogeneous distribution so that the loaded polymer chains can be sequentially detached (or fractured) to gradually dissipate the stored elastic energy. In addition, different from the permanent covalent bonds in the organically crosslinked hydrogels, the bonding between the nanoparticle crosslinkers and the polymer chains are through physical bonds such as ionic and coordination interactions (Carlsson et al., 2010; Haraguchi and Takehisa, 2002). When deformed, a portion of polymer chains can detach from the nanoparticle crosslinkers to partially release the stored elastic energy in the polymer network. Because of the high energy dissipation, this nanocomposite hydrogel exhibits extraordinarily higher stretchability and toughness than the conventional covalently crosslinked hydrogel, thus showing great potential to be used in the artificial muscles and cartilages (Haraguchi, 2011b).

Despite the great potential, the mechanistic mechanisms underlying the mechanical performance of the nanoparticle hydrogels have not been well quantitatively investigated. Balaz et al., employed molecular dynamic computations to study the mechanical deformation and strain recovery of the nanoparticle crosslinked polymer networks (Iyer et al., 2014, 2013).

Due to the limited computational size scales, it is unclear how well the computational results match the macroscopic stress–strain behaviors of the nanoparticle hydrogels. In particular, it is highly desirable to construct a simple analytical model, in order to fully utilize the premium mechanical properties or guide/promote the further development of this type of nanoparticle hydrogels (Iyer et al., 2014, 2013). In addition, we note that the theoretical development of the nanoparticle hydrogels is different from that of the well-studied filled elastomers; because the nanoparticle hydrogels only contain nanoparticle crosslinkers, but filled elastomers mainly have organic crosslinkers from the backbone elastomers and only include a small portion of additional filler crosslinkers (Bueche, 1960; Dargazany and Itskov, 2009; Diani et al., 2009; Govindjee and Simo, 1991; Haraguchi et al., 2006). Besides, the nanoparticle hydrogels embed water within the polymer network structures. Moreover, unlike the hydrogels with traditional covalently-crosslinked networks that have been well modeled with Neo-Hookean model, 3-chain model, 4-chain model, 8-chain model and n-chain model (Erman and Mark, 1997; Flory, 1953; Rubinstein and Colby, 2003; Treloar, 1975), it is still elusive how to mechanistically bridge the relationship between the molecular structure of nanoparticle crosslinked polymer networks of the nanoparticle hydrogels and their mechanical properties. In particular, It is largely elusive how to relate the chain length inhomogeneity (Wang et al., 2015; Zhao, 2012) and deformation induced chain evolution to the experimentally observed stress–strain hysteresis of the nanoparticle hydrogels (Haraguchi, 2011b; Haraguchi and Takehisa, 2002; Iyer et al., 2014, 2013).

Here we formulate a constitutive model to understand the stress–strain behaviors of nanoparticle hydrogels. We model the polymer network with polymer chains with inhomogeneous length crosslinked with nanoparticles that are arranged in shape of body-centered cubes. We assume that the polymer chains can detach from the nanoparticles if the chain forces are larger than the bonding strength between the particle and the polymer chain. Once detached, the polymer chains will reorganize and evolve. Considering the effects of chain detachment and evolution enables us to model the Mullins effect of the nanoparticle hydrogels (Mullins and Tobin, 1965). Experiments with a model hydrogel with silica nanoparticles as crosslinkers can quantitatively validate our theory. The constitutive model can also be used to explain the cyclic stress–strain behaviors of nanoclay hydrogels that only use nanoclays as crosslinkers. The model can be further extended to explain the experimentally observed necking instability of hydrogels with both nanoparticle and organic crosslinkers.

The plan of the paper is as follows. Section 2 introduces the experimental procedures of the fabrication and mechanical testing of the nanoparticle hydrogels. Section 3 presents a constitutive model that considers the architecture and evolution of the polymer networks of the nanoparticle hydrogels under large deformation. Based on the constructed constitutive model, in Section 4 we examine the effects of chain detachment, chain alteration, particle concentration and particle size on the stress–strain behaviors of the nanoparticle hydrogels. Theoretical predictions are quantitatively compared with the experimentally measured results of nanosilica hydrogels. In Section 5, we show applications of the established theory in predicting the mechanical behaviors of nanoclay hydrogels. We further extend the theory to explain the necking instability of nanocomposite hydrogels with both nanoparticle and organic crosslinkers. The conclusive remarks are given in Section 6.

2. Experimental

Here we choose silica nanoparticles as crosslinkers to polymerize polymer monomers N,N-Dimethylacrylamide (DMA, Siglma-Aldrich) or N-Isopropylacrylamide (NIPA, Siglma-Aldrich) within aqueous solutions because the polymerization can take place at room temperature (25 °C) (Carlsson et al., 2010), advantageous over the fabrication of other nanoparticle hydrogels (e.g., nanoclay hydrogels) that requires low temperature condition (≤ 5 °C) (Haraguchi, 2011b; Haraguchi and Takehisa, 2002). To initiate the free-radical polymerization between the polymer chains and silica nanoparticles, we use potassium persulfate (KPS, Siglma-Aldrich) as the redox initiator and *N,N,N′,N′*-tetramethylethylenediamine (TEMED, Siglma-Aldrich) as the accelerator. For all hydrogels, we keep the molar ratio of DMA, KPS and TEMED as 100:1:1, and the weight ratio of DMA and water as 0.14. To examine the effects of the nanoparticle concentrations on the stress–strain behaviors of the nanocomposite hydrogels, the weight ratio of DMA and silica nanoparticles is varied to be 1, 2 and 5, denoted as SP1, SP2 and SP5, respectively (Carlsson et al., 2010). To study the effects of nanoparticle sizes on the gel stress–strain behaviors, we employ silica nanoparticles with varied sizes, i.e., TM-50 (50% wt particle suspension) with radius 7.5 nm, HS-40 (40% wt particle suspension) with radius 4.5 nm and SM-30 (30% wt particle suspension) with 2.5 nm (Rose et al., 2014). We denote the fabricated hydrogels as TM-SPX, HS-SPX and SM-SPX (X denotes 1, 2 or 5), respectively. The detailed compositions of fabricated hydrogels are listed in Table 1. In a typical fabrication process of TM-SP2 hydrogels,

Table 1
Compositions of nanocomposite hydrogels with nanosilica crosslinkers.

Sample	Nanosilica suspension	Silica (g)	DI water (g)	DMA (g)	KPS (g)	TEMED (μL)
TM-SP1	TM-50	1.428	10.555	1.485	0.0405	20
TM-SP2	TM-50	2.856	10.555	1.485	0.0405	20
TM-SP5	TM-50	7.14	10.555	1.485	0.0405	20
HS-SP2	HS-40	2.856	10.555	1.485	0.0405	20
SM-SP2	SM-30	2.856	10.555	1.485	0.0405	20

7.699 g DI water and 5.712 g Ludox TM-50 (Sigma-Aldrich) in a plastic tube are mixed with Vortex for 30 min. Then, 1.485 g DMA, 0.0405 KPS and 22.5 μL TEMED are added into the plastic tube with additional mixing for 45 min. Finally, we transfer the hydrogel solution into a glass mold (length 75 mm, width 45 mm and height 4 mm) for polymerization overnight. Once polymerized, the hydrogels are cut into pieces with dimension length 37 mm, width 45 mm and height 4 mm and mounted on a stress–strain tester (Model 5942, Instron). The clamped samples with initial gauge length 4 mm, width 45 mm and thickness 4 mm are uniaxially stretched with low strain rate $\sim 0.06\ s^{-1}$ and unloaded with strain rate $-0.06\ s^{-1}$. To demonstrate the high toughness of the hydrogel samples, we cut a crack with length around 4 mm (along width direction) in the sample center (Fig. 1c). As shown in Fig. 1c, the hydrogel (TM-SP2 hydrogel) with a center crack can be stretched for 44 times of the original length.

3. The constitutive model

3.1. The free energy function

The nanoparticle hydrogel consists of nanoparticle-crosslinked polymer networks and water. The free energy of the hydrogel comes from two parts: stretching the polymer network and the mixing between the polymer chains and water molecules (Flory and Rehner Jr., 1943; Hong et al., 2008). Therefore, the free energy of the nanoparticle hydrogel per unit reference volume can be expressed as,

$$W = W_s + W_m \tag{1}$$

where W_s and W_m are free energy density due to stretching the polymer networks, and mixing polymer chains and water molecules, respectively. The mixing free energy has been modeled by Flory and Rehner by considering the polymer solvent interactions (Flory and Rehner Jr., 1943; Hong et al., 2008). During the mechanical testing of the nanoparticle hydrogel, the nominal water concentration of the hydrogel is kept nearly constant (no contact with water and carefully control the moisture) and the temperature remains at room temperature (25 °C). In addition, the water diffusion time scale ($\sim (0.04\ m)^2/1 \times 10^{-6}\ m^2\ s^{-1} \sim 27$ min) within the hydrogel is usually much larger than the experimental time scale in the current paper (loading ~ 2.5 min). Therefore, we assume that the mixing free energy density of the nanoparticle hydrogel W_m remains constant throughout the mechanical deformation.

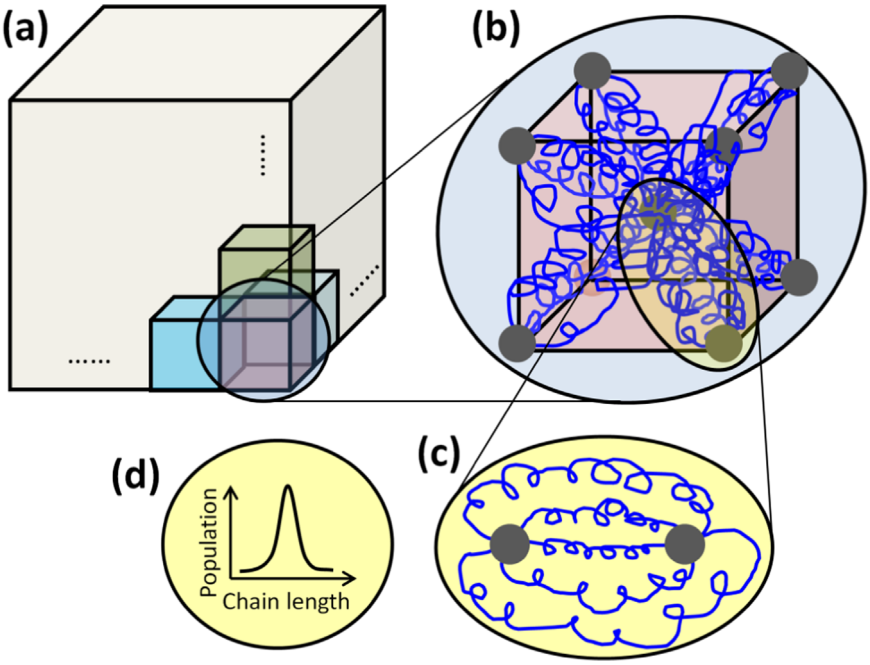

Fig. 2. Proposed network model of the nanocomposite hydrogel. (a) The hydrogel consists of layered body-centered cubes. (b) Particle crosslinkers are located on the corners and the center of the cube. (c) Between a particle pair, polymer chains with (d) inhomogeneous lengths are attached on the particle surfaces.

3.2. The network model

3.2.1. The fabricated hydrogel network

In a nanoparticle hydrogel, the nanoparticles act as crosslinkers to bridge the polymer chains into a polymer network through the ionic and coordination interactions between nanoparticles and the polymer chains (Haraguchi and Takehisa, 2002). For example, the anionic groups of the polymer chains can be ionically bonded to SO_3^- and K^+ groups which come from the redox initiator KPS and are attached on the nanoparticle surface. Due to the large aspect area of the nanoparticles, the nanoparticle surfaces may have a large number of attaching groups (e.g., >100) which bond a large number of polymer chains on one nanoparticle crosslinker. The nanoparticles, hooked by the polymer chains, in turn are self-assembled into a three-dimensional architecture. Experiments with Transmission Electron Microscopy have verified that the nanoparticles within the polymer networks indeed layout as a three-dimensional periodic architecture with average particle–particle distance (Williams et al., 2015). Between two particles, the attached polymer chains usually do not have the same chain length, but have inhomogeneous chain lengths over a wide distribution (Haraguchi, 2011b; Haraguchi and Takehisa, 2002; Zhao, 2014). This chain inhomogeneity contributes to the high toughness of the nanoparticle hydrogels in that large deformation may first break short polymer chains to partially dissipate elastic energy, while the long polymer chains can still maintain the elasticity of the hydrogels.

In the current paper, we try to develop a simplest network model to capture the essential polymer network architecture and polymer chain length inhomogeneity. To simplify the model, we assume that the elasticity of the network only come from the crosslinking between the polymer chains and the nanoparticle surfaces, without considering the interaction or entanglement of the polymer chains. Following the essential idea of polymer network models (Erman and Mark, 1997; Rubinstein and Colby, 2003; Treloar, 1975), we assume that the network is constructed by layering a number of unit cubes to span over the whole volume of the hydrogel (Fig. 2a). In each unit cube, nanoparticles are located on the corners and centers in a body-centered fashion: 8 nanoparticles on corners and 1 nanoparticle in the center of the cube (Fig. 2b). One corner particle and the center particle form a particle pair, and a number of polymer chains attach between the particle pair (Fig. 2c). The polymer chains between a particle pair do not have the uniform chain length, but follow a non-uniform chain-length distribution function (Fig. 2d).

For a fabricated hydrogel, we assume the particle concentration (the number of particles per unit volume of the fabricated hydrogel) as η_p. Since each cube averagely occupies 2 particles (Fig. 2b), the volume of each cube can be calculated as

$$v_u = \frac{2}{\eta_p} \tag{2}$$

The size of the cube can be calculated as

$$a = (v_u)^{\frac{1}{3}} = \left(\frac{2}{\eta_p}\right)^{\frac{1}{3}} \tag{3}$$

The distance between the center and the corner particles (distance of a particle pair) can thus be written as

$$D = \frac{\sqrt{3}}{2}a = \frac{\sqrt{3}}{2}\left(\frac{2}{\eta_p}\right)^{\frac{1}{3}} \tag{4}$$

Each unit cube with volume v_u occupies 8 particle–particle pairs. The number of particle–particle pairs in a unit volume of the hydrogel is

$$\eta_{pair} = \frac{8}{v_u} = 4\eta_p \tag{5}$$

Between each particle pair, we assume that N polymer chains with inhomogeneous chain lengths are attached on the nanoparticles. Each polymer chain is describe by the Kuhn's polymer theory; that is, a polymer chain is made of a number of freely jointed Kuhn segments with each segment length b (taken as 1.1×10^{-10} m through the paper) (Erman and Mark, 1997; Rubinstein and Colby, 2003; Treloar, 1975). We assume that the polymer chains can be classified to m types of chains, each type with the same Kuhn segment number. We denote the Kuhn segment number (chain length) of the ith polymer chain as n_i, and the number of ith polymer chains as N_i, where $1 \le i \le m$. Without loss of generality, we further assume $n_1 \le n_2 \le \ldots n_i \ldots \le n_m$. Therefore, the number of total polymer chains between a particle pair can be calculated as

$$N = \sum_{i=1}^{m} N_i \tag{6}$$

The number of the ith polymer chain follows a statistical probability distribution as

$$P_i(n_i) = \frac{N_i}{N} \tag{7}$$

where the summation of the probability densities should be equal to a unit, i.e., $\sum_{i=1}^{m} P_i(n_i) = 1$. The probability density function $P_i(n_i)$ will be discussed in details in Section 3.4.

Since we assume each of the ith chains is freely jointed with n_i Kuhn segments, the fully extended contour length of the ith chain is $r_i^c = n_i b$. In the freely joint state, the average end-to-end distance can be approximated as the root-mean-square distance of the freely jointed Kuhn segments, namely

$$r_i^0 = \sqrt{n_i} b \tag{8}$$

Under deformation, the end-to-end distance of the ith chain becomes r_i, and the stretch of the ith chain can be expressed as

$$\Lambda_i = \frac{r_i}{r_i^0} \tag{9}$$

where the chain stretch must be in a range, $0 \le \Lambda_i \le r_i^c / r_i^0 = \sqrt{n_i}$. Assuming the particle size is small, we approximate the end-to-end distance of ith chain as the particle distance Dat the fabricated state, i.e., $r_i = D$.

According to Langevin-chain statistics (Kuhn and Grün, 1942), the chain force on the ith chain at the fabricated state can be expressed as

$$f_i = \frac{k_B T}{b} L^{-1}\left(\frac{r_i}{n_i b}\right) = \frac{k_B T}{b} L^{-1}\left(\frac{D}{n_i b}\right) \tag{10}$$

where $L^{-1}()$ is the inverse Langevin function, and the Langevin function can be written as $L(x) = \coth x - 1/x$.$k_B = 1.38 \times 10^{-23}$ m^2 kg s^{-2} K^{-1}is Boltzmann constant, and T is the absolute temperature in Kelvin. It can be seen from Eq. (10), the chain force becomes smaller as increasing the chain length and the chain becomes more flexible. Among all chains attached on the particle pair, the largest chain force exists on the first type of chain with Kuhn number n_1, i.e.,

$$f_1 = \frac{k_B T}{b} L^{-1}\left(\frac{D}{n_1 b}\right) \tag{11}$$

If n_1 is small enough, the bonding between the polymer chain and the nanoparticle may not be able to sustain the large tensile chain force. We assume the bonding strength between the polymer chain and the nanoparticle as f_{str}. The smallest Kuhn segment number of a polymer chain (i.e., chain length n_1 of the first type of the chain) between the particle pair can thus be calculated as

$$n_1 = \frac{1}{L\left(\frac{f_{str} b}{k_B T}\right)} \frac{D}{b} = \frac{1}{\coth\left(\frac{f_{str} b}{k_B T}\right) - \frac{k_B T}{f_{str} b}} \frac{D}{b} \tag{12}$$

The Kuhn segment number of other types of polymer chains should be larger than n_1, i.e., $n_1 \le n_2 \le \ldots n_i \ldots \le n_m$, where n_m is the largest Kuhn segment number.

3.2.2. *The deformed hydrogel network with chain evolution*

When the fabricated hydrogel is under macroscopic mechanical deformation, the distance of the particle pair increases

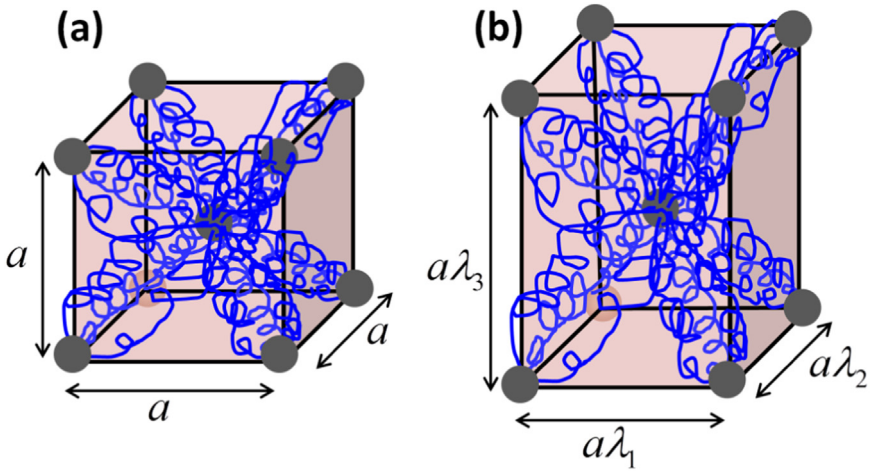

Fig. 3. Deformation of a body-centered unit cube follows the affined deformation assumption with stretches in three directions (λ_1, λ_2 and λ_3) the same as those of the macroscopic deformation.

and the polymer chains are elongated. At the fabricated state, the side lengths of the body-centered cube are $a \times a \times a$ and the distance of the particle pair is $D = \sqrt{3}a/2$(Fig. 3). At the current state, the hydrogel is under three directional stretch λ_1, λ_2 and λ_3. We assume that the deformation of the body-centered cube follows the affined deformation assumption (Arruda and Boyce, 1993; Rubinstein and Colby, 2003; Treloar, 1975), and is thus deformed by λ_1, λ_2 and λ_3 in three directions (Fig. 3). Therefore, the distance of the particle pair becomes

$$d = \frac{\sqrt{\lambda_1^2 + \lambda_2^2 + \lambda_3^2}}{2} a = \sqrt{\frac{I_1}{3}} D \tag{13}$$

where $I_1 = \lambda_1^2 + \lambda_2^2 + \lambda_3^2$ is the first invariant of right Cauchy Green tensor. The stretch of the particle pair is

$$\Lambda_{pair} = \frac{d}{D} = \sqrt{\frac{I_1}{3}} \tag{14}$$

Taking the fabricated state as the reference state, we can write the relative stretch of the ith chain as

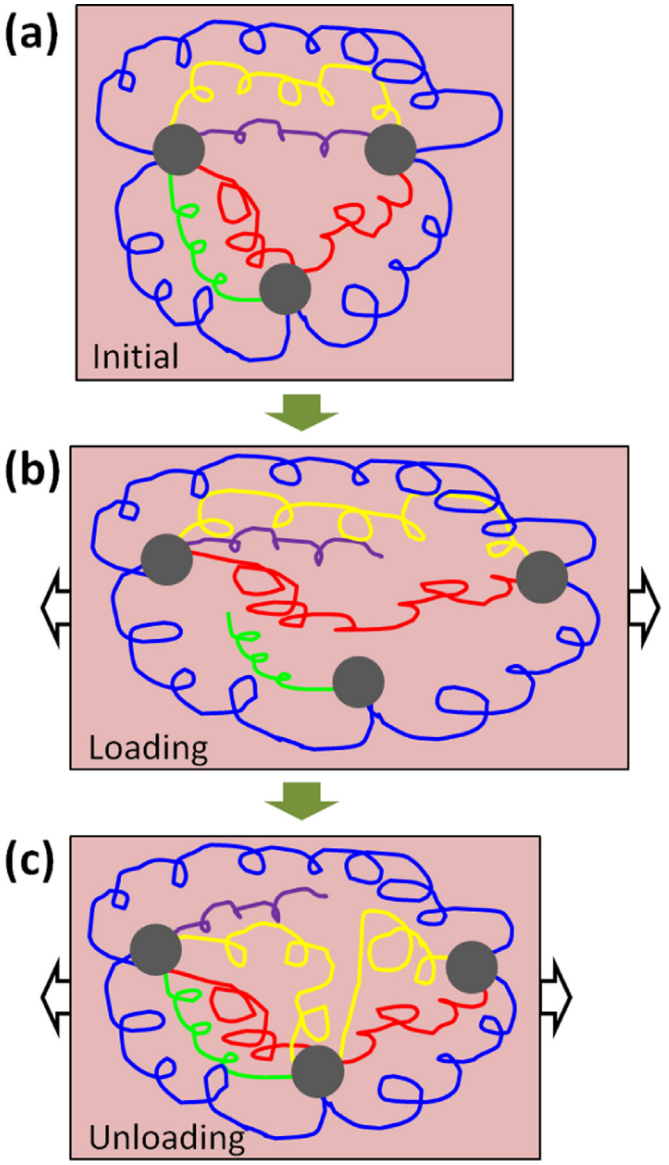

Fig. 4. Evolution of the polymer network of the nanocomposite hydrogel. (a) The polymer network at the reference state. (b) Under loading, polymer chains can be detached from the particles to be either inactive (green and purple chains) or become longer active chains (red chains). (c) Under unloading, long chains can graft on the middle particles (red and yellow chains), and previously detached short chains can also be re-attach on the particles (green chain). (For interpretation of the references to color in this figure legend, the reader is referred to the web version of this article.)

$$\Lambda_i = \frac{d}{D} = \sqrt{\frac{I_1}{3}} \tag{15}$$

It is also noted that if we take the freely-relaxed state as the reference state, the real stretch of the ith chain is $(\Lambda_i D)/(\sqrt{n_i}b)$. By assuming the particle size is small, we can approximate the end-to-end distance of ith chain as the particle distance d at the current state. The chain force on the ith chain at the current state is (Kuhn and Grün, 1942)

$$f_i = \frac{k_B T}{b} L^{-1}\left(\frac{r_i}{n_i b}\right) = \frac{k_B T}{b} L^{-1}\left(\frac{D}{n_i b}\sqrt{\frac{I_1}{3}}\right) \tag{16}$$

Upon the mechanical loading of the hydrogel, a number of polymer chains can be detached from the particles (Fig. 4ab). Upon the mechanical unloading, these detached polymer chains may be re-attached or re-organized (Fig. 4c). The microscopic chain evolution leads to stretch-induced softening and the hysteresis of the cyclic stress–strain behaviors, so called Mullins effect (Carlsson et al., 2010; Haraguchi, 2011b; Mullins and Tobin, 1965). A number of theories have been proposed to study the Mullins effect of elastomers and hydrogels, such as domain evolution theory (Johnson and Beatty, 1993; Mullins and Tobin, 1965; Qi and Boyce, 2004), damage theory (Blanchard and Parkinson, 1952; Bueche, 1960; Govindjee and Simo, 1991; Lion, 1996), network alteration theory (Chagnon et al., 2006; Marckmann et al., 2002; Zhao, 2012) and phenomenological theory (Dorfmann and Ogden, 2003; Miehe, 1995; Ogden and Roxburgh, 1999). Here, we study the Mullins effects of particle hydrogel network by considering the chain detachment and evolution during the mechanical loading–unloading. The goal is to use the simplest model to capture the network evolution process of the stressed nanocomposite hydrogels and elucidate the physical essence of the Mullins effects of the nanocomposite hydrogels under large deformation.

We assume that during the loading–unloading history the hydrogel undergoes largest deformation denoted with the maximum of the first invariant of right Cauchy Green tensor, i.e.,

$$I_{\max} = \left(\lambda_1^2 + \lambda_2^2 + \lambda_3^2\right)_{\max} \tag{17}$$

The corresponding largest relative stretch and largest chain force of the ith chain respectively are

$$\left(\Lambda_i\right)_{\max} = \sqrt{\frac{I_{\max}}{3}} \tag{18}$$

$$\left(f_i\right)_{\max} = \frac{k_B T}{b} L^{-1}\left[\frac{D}{n_i b}\sqrt{\frac{I_{\max}}{3}}\right] \tag{19}$$

3.2.2.1. The chain detachment. When the hydrogel is under virgin mechanical loading with I ($I = I_{\max}$), the tensile chain force on the ith chain f_i is given in Eq. (16). If f_i is equal to or larger than the maximum attachment strength on the particles f_{str}, the ith chain will be detached from the particles (e.g., purple and green chains in Fig. 4b). Here we consider the bonding between the polymer chain and particles is physical bonding, we thus assume that the attachment strength is much smaller than the fracture strength of the polymer chain, and we only consider chain detachment without chain fracture (Haraguchi, 2011b; Haraguchi and Takehisa, 2002). Due to chain detachment, the short chains will be detached, leaving only long chains attaching between particles. The critical chain length can be calculated by

$$f_i = \frac{k_B T}{b} L^{-1}\left(\frac{D}{n_i b}\sqrt{\frac{I_1}{3}}\right) = f_{str} \tag{20}$$

We thus can calculate the critical chain length n_c as

$$n_c = \frac{1}{L\left(\frac{f_{str} b}{k_B T}\right)} \frac{D}{b}\sqrt{\frac{I_1}{3}} \tag{21}$$

where $n_c \geq n_1$ and n_c is the chain length of the cth type of chain ($c \geq 1$). It can be seem from Eq. (21), the critical chain length n_c increases with the strain invariant I_1. During the load–unloading history, the maximum critical chain length is

$$n_{mc} = \frac{1}{L\left(\frac{f_{str} b}{k_B T}\right)} \frac{D}{b}\sqrt{\frac{I_{\max}}{3}} \tag{22}$$

where n_{mc} is the chain length of the mcth type of chain.

After chain detachment, the length of the active chains should be always larger than n_c, i.e., $n_c \leq n_{c+1} \ldots \leq n_m$. The number of active chains between a particle pair can be expressed as

$$N_a = \sum_{i=c}^{m} N_{ia} = \sum_{i=c}^{m} P_i N \tag{23}$$

where $N_{ia} = P_i N$is the number of the active ith polymer chains ($i \geq c$).

3.2.2.2. The network alteration. During the mechanical loading (virgin loading with $I_1 = I_{\max}$ or non-virgin loading with $I_1 \leq I_{\max}$), a portion of detached short chains may become active long chains (illustrated as the red chain from Fig. 4a to b). To capture this effect, we follow the network alteration theory to model the number of the active chains to be an exponential function with the chain stretch as (Chagnon et al., 2006; Marckmann et al., 2002; Ogden and Roxburgh, 1999; Zhao, 2012)

$$\frac{N_{ia}}{N_i} = \exp\left[\alpha_1\left(\sqrt{\frac{I_{\max}}{3}} - 1\right)\right] \tag{24}$$

where N_{ia} is the active chain number of the ith chains after the network alteration, α_1 is a positive parameter, and $c \leq i \leq m$. It is noted that during the virgin loading $I_{\max}$ in Eq. (24) is equal to I_1, while $I_{\max} \geq I_1$ during the non-virgin loading.

During the mechanical unloading with $I < I_{\max}$, a number of polymer chains can reorganize or re-attach on the particles. First, during the mechanical unloading the stretched long chains may become relaxed and may graft on the middle particles (see red and yellow chains in Fig. 4c); therefore, the long chain number may decrease by a portion. We model the long chain grafting during the unloading as (Chagnon et al., 2006; Marckmann et al., 2002; Ogden and Roxburgh, 1999; Wang and Hong, 2011; Zhao, 2012)

$$\frac{N_{ia}}{N_i} = \exp\left[\alpha_1\left(\sqrt{\frac{I_{\max}}{3}} - 1\right)\right]\exp\left[-\alpha_2\left(\sqrt{\frac{I_{\max}}{3}} - \sqrt{\frac{I_1}{3}}\right)\right] \tag{25}$$

where α_2 is a positive parameter, and Eq. (25) is only for the long chains with chain length $n_{mc} \leq n_i \leq n_m$.

Second, the long chain grafting during unloading can in turn contribute to the increasing of shorter chains with chain length $n_c \leq n_i < n_{mc}$. In addition, the re-attachment of the detached shorter chains ($n_c \leq n_i < n_{mc}$) can also increase the number of these short chains (green chain in Fig. 4c). Following a similar exponential function as Eq. (25), we model the short chain number restoration as (Chagnon et al., 2006; Marckmann et al., 2002; Ogden and Roxburgh, 1999; Wang and Hong, 2011; Zhao, 2012)

$$\frac{N_{ia}}{N_i} = \exp\left[-\alpha_3\left(\sqrt{\frac{I_{\max}}{3}} - \sqrt{\frac{I_1}{3}}\right)\right] \tag{26}$$

where Eq. (26) is only for $n_c \leq n_i < n_{mc}$. α_3 can be positive with $N_{ia} < N_i$ or negative with $N_{ia} > N_i$.

3.3. Stress–stretch relationship

The free energy of deforming the hydrogel network comes from the free energy of deforming all polymer chains between the particle pairs. Since the particle volume fraction is very small, we assume that the effect of nanoparticles on the overall free energy of the hydrogel is negligible. In a unit reference volume of the hydrogel, the particle pair number is $\eta_{pair} = 4\eta_p$ (Eq. (5)). Therefore, the free energy of the polymer network per unit volume of the deformed hydrogel can be calculated as

$$W_s = 4\eta_p \sum_{i=c}^{m} \left[\omega_i(n_i, \Lambda_i) N_{ia}\right] \tag{27}$$

where N_{ia} is the number of active ith chain given in Eqs. (25)–(27) during the mechanical loading or unloading, and the free energy of the deformed ith chain can be calculated by (Kuhn and Grün, 1942)

$$\omega_i(n_i, \Lambda_i) = n_i k_B T\left[\frac{\beta_i}{\tanh \beta_i} + \ln\left(\frac{\beta_i}{\sinh \beta_i}\right)\right] \tag{28}$$

where $\beta_i = L^{-1}(\frac{r_i}{n_i b}) = L^{-1}(\frac{\Lambda_i D}{n_i b})$, $L^{-1}()$ is the inverse Langevin function, and $\Lambda_i = \sqrt{I_1/3}$ given by Eq. (15).

It is noted that in Eq. (28) we assume that any polymer chains with the same length, including initially-attached and reattached chains, have the same stretching free energy at a certain macroscopic strain invariant I_1. It is understood in the following way. Under mechanical loading, when the chain force f_i of the ith chain is larger than the attaching strength f_{str}, the polymer chain is detached from the particle. Once detached, the stretching free energy of this polymer chain is not counted into the total stretching free energy of the network. However, it does not mean that the polymer chain spontaneously relaxes the end-to-end distance back to $\sqrt{n_i} b$, because this relaxation process within a solid hydrogel matrix takes time. The chain length relaxation process is usually modeled by de Gennes' reptation model (de Gennes, 1971; Rubinstein and Colby, 2003) which gives the chain diffusion coefficient as $D_c = (k_B T)/(n_i \varsigma)$, where ς is the friction coefficient per Kuhn segment. Therefore, the chain relaxation time scale can be estimated as $(d - \sqrt{n_i} b)^2/D_c$, where d is the particle distance when

the polymer chain is detached. If we input some characteristic values for the parameters, such as $n_i = 1000$, $d = 4D = 400b$, $b = 1.1 \times 10^{-10}$ m, and $\varsigma \approx 1 \times 10^{-5}$ kg s^{-1} (de Gennes, 1971; Rubinstein and Colby, 2003), the chain relaxation time can be estimated as 66 min that is much larger than the experimental time scale (loading–unloading ~5 min). Under this assumption, we argue that during the period between the detaching and unloading-reattaching, the polymer chain probably nearly unchanges the end-to-end distance. When the hydrogel is unloaded, the polymer chain probably re-attaches back to the particle (reflected by Eq. (26)) with nearly unchanged end-to-end distance.

We assume that the hydrogel network is incompressible. Since we fix the free energy density due to the mixing W_m to be constant, we can write the principal stress as

$$\sigma_1 = \lambda_1 \frac{\partial W_s}{\partial \lambda_1} - \Pi \tag{29a}$$

$$\sigma_2 = \lambda_2 \frac{\partial W_s}{\partial \lambda_2} - \Pi \tag{29b}$$

$$\sigma_1 = \lambda_3 \frac{\partial W_s}{\partial \lambda_3} - \Pi \tag{29c}$$

where Π is the hydrostatic pressure to enforce the incompressibility.

If we consider a pure-shear uniaxial tension, the uniaxial stretch is $\lambda_1 = \lambda$ and the transverse stretches are $\lambda_2 = \lambda^{-1}$ and $\lambda_3 = 1$ (Fig. 1ci–cii). By considering the stresses in transverse directions vanish, the true stress in the uniaxial tension direction can be derived as

$$\sigma_1 = 4\eta_p k_B T \frac{D}{b}\left(\lambda^2 - \lambda^{-2}\right) \sum_{i=c}^{m} \left(\frac{N_{ia}\beta_i}{\sqrt{3I_1}} \right) \tag{30}$$

The nominal stress can thus be written as

$$s_1 = 4\eta_p k_B T \frac{D}{b}\left(\lambda - \lambda^{-3}\right) \sum_{i=c}^{m} \left(\frac{N_{ia}\beta_i}{\sqrt{3I_1}} \right) \tag{31}$$

Similarly, if we consider a uniaxial tension with $\lambda_1 = \lambda$ and $\lambda_2 = \lambda_3 = \lambda^{-1/2}$, the nominal stress along the stretching direction can be calculated as

$$s_1 = 4\eta_p k_B T \frac{D}{b}\left(\lambda - \lambda^{-2}\right) \sum_{i=c}^{m} \left(\frac{N_{ia}\beta_i}{\sqrt{3I}} \right) \tag{32}$$

3.4. Chain length distribution

We consider the length distribution of the polymer chains bridging two particles by following Bueche (1960). Between a particle pair, N polymer chains are attached on with Kuhn segment $n_1 \le n_2 \le \ldots n_i \ldots \le n_m$. Assuming the particle is small, we approximate the end-to-end distance of ith chain as the particle distance D at the fabricated state. Following Gaussian statistics, if one end of ith chain is attached to one particle surface, the chance that n_ith Kuhn segment along the ith chain is within a distance ΔD of position D can be considered as a 1D random-walk problem (Fig. 5), with the probability expressed as (Bueche, 1960; Flory, 1953; Rubinstein and Colby, 2003; Treloar, 1975),

$$P_1 = \left(\frac{3}{2\pi n_i b^2} \right)^{\frac{1}{2}} \exp\left(-\frac{3D^2}{2n_i b^2} \right) \Delta D \tag{33}$$

where the Kuhn length is b and n_i is the Kuhn segment number of the ith chain. It is noted that this 1D random walk model is different from commonly used 3D random walk model for 3D behaviors of a polymer chain. This 1D random walk model is

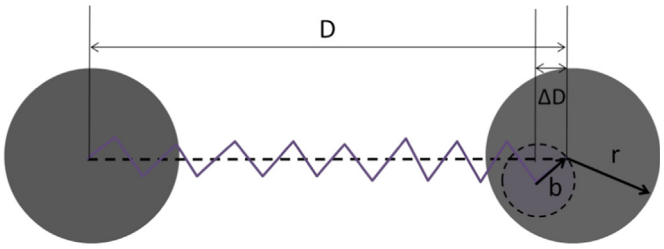

Fig. 5. Chain attaching model between a particle pair.

valid because we only consider the chain-length distribution between two particles (Bueche, 1960); however, 3D random walk model may involve more than one particle pair (e.g., 8 particle pairs in the current situation). This 1D random walk model to formulate the chain length distribution between a particle pair has been widely accepted and adopted (Bueche, 1960; Dargazany and Itskov, 2009; Diani et al., 2009; Govindjee and Simo, 1991).

When looking closer into the n_ith segment, we consider the thermal-driven random motion of the n_ith segment actually induces perturbation around a small volume (Fig. 5). This small volume can be approximated as a sphere with radius b. We further assume the random motion of the n_ith segment coincides with the perturbation ΔD of the ending point of the chain. Therefore, we can approximate the perturbation distance ΔD the n_ith Kuhn segment around the position D as

$$\Delta D \approx b \tag{34}$$

We denote the chance that the n_ith Kuhn segment (spanning ΔD around the position D) can attach on the particle surface as κ. We calculate κ in the following way. We assume the radius of the particle as r. On each particle surface, N_{site} active sites exist to form ionic or coordination interactions with the polymer chains. The number of such active site highly depends on the deposition of the redox initiator upon the particle surface. On the particle surface, the average area per active site is thus written as

$$A_{site} = \frac{4\pi r^2}{N_{site}} \tag{35}$$

The probability that the n_ith Kuhn segment with a length b can attach on such active site can be approximated as the ratio between the spanning area of the n_ith Kuhn segment (Fig. 5) and the area of one active site, i.e.,

$$\kappa = \frac{\pi b^2}{A_{site}} = \frac{b^2 N_{site}}{4r^2} \tag{36}$$

where we can also callκas the activity of the particle surface. The particle surface activity increases monotonically with the number of active sites on the particle surface, and decreases with the particle size r.

Based on Eqs. (33)–(36), we can calculate the probability that n_ith Kuhn segment of the ith chain attach on another particle surface (one end has attached on one particle surface) is

$$P_2 = P_1\kappa = b\kappa\left(\frac{3}{2\pi n_i b^2}\right)^{\frac{1}{2}} \exp\left(-\frac{3D^2}{2n_i b^2}\right) \tag{37}$$

Here, we consider two ends of the ith chain attach on two particles and we thus should also exclude the situation that the middle Kuhn segments attach on particle surfaces. The probability shorter Kuhn segments (1st to (n_i-1)th) cannot attach to the particle surface can be expressed as

$$P_3 = \prod_{s=1}^{n_i-1}\left[1 - b\kappa\left(\frac{3}{2\pi s b^2}\right)^{\frac{1}{2}} \exp\left(-\frac{3D^2}{2s b^2}\right)\right] \tag{38}$$

In is noted that if a polymer chain attach on a particle via a middle Kuhn segments, rather than the ending segments, the polymer chain should be treated as two chains with shorter lengths, respectively. Combining Eqs. (37) and (38), we can compute the probability that the ith chain with Kuhn number n_i attach on a particle pair with distance D as

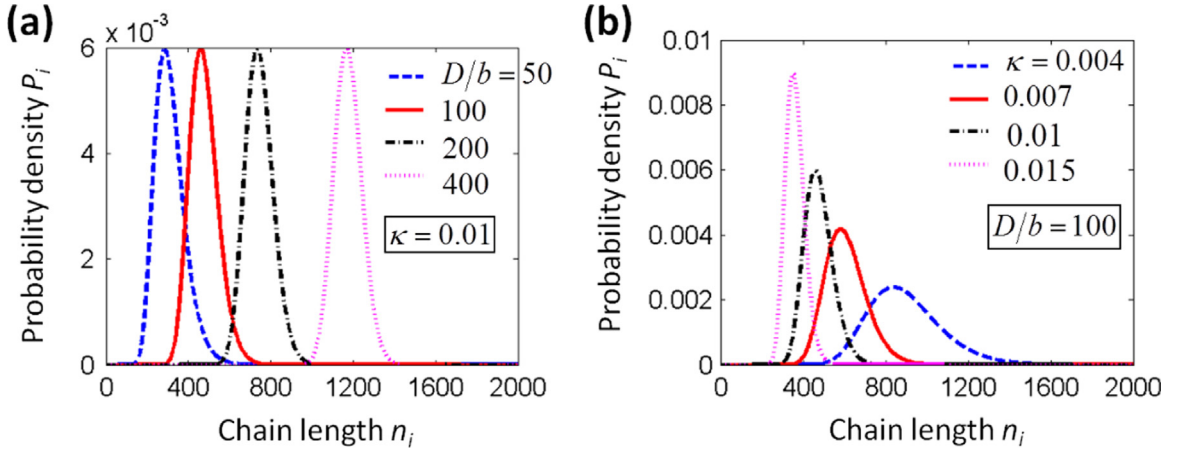

Fig. 6. Probability densities $_{Pi}$ plotted as functions of chain lengths n for varied (a) particle distances D/b and (b) particle activity κ.

$$P_4(n_i) = P_2 P_3 \tag{39}$$

Eq. (39) can be explicitly written as (Dargazany and Itskov, 2009; Govindjee and Simo, 1991),

$$P_4(n_i) = \kappa\left(\frac{3}{2\pi n_i}\right)^{\frac{1}{2}} \exp\left\{-G - \frac{\kappa}{\sqrt{\pi}}\left[\sqrt{6n_i}e^{-G} + 3\frac{D}{b}\sqrt{\pi n_i}\,erf\left(\sqrt{G}\right) - \sqrt{6}e^{-Gn_i} - 3\frac{D}{b}\sqrt{\pi}\,erf\left(\sqrt{Gn_i}\right)\right]\right\} \tag{40}$$

where $G = 3D^2/(2n_i b^2)$. To normalize $P_4(n_i)$, we enforce a factor $\bar{P}$ to obtain $P_i(n_i)$ in Eq. (7), i.e.,

$$P_i(n_i) = P_4(n_i)\bar{P} \tag{41}$$

so that the summation of $P_i(n_i)$ equals to a unit, i.e., $\sum_{i=1}^{m} P_i(n_i) = 1$.

From Eqs. (40) and (41), we can see that the chain length distribution density $P_i(n_i)$ is a function of particle pair distance D/b and the activity of the particle surface κ. With increasing chain length, the probability density increases first and then decreases with a highest probability at the median chain length. The larger the particle pair distance, the more long chains can attach on the particles. Therefore, the chain length with the highest probability increases with the increasing particle pair distance D/b (Fig. 6a). Moreover, with the higher activity of the particles, it is more probable that the polymer chains with chain length of wider distributions. As shown in Fig. 6b, increases with the particle activity κ the half-height width of the probability distribution increases.

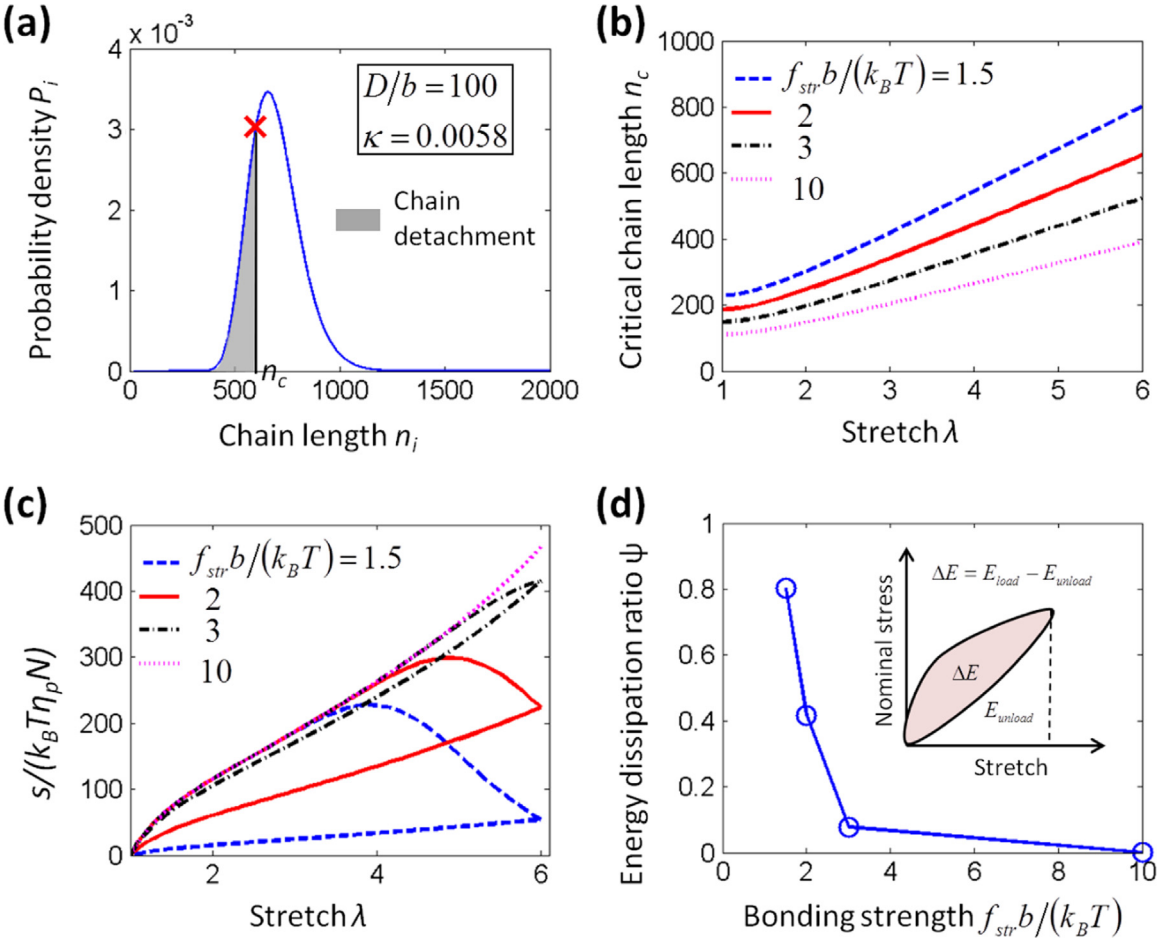

Fig. 7. Effect of chain detachment on the stress–stretch behaviors of the nanocomposite hydrogels. (a) The probability density plotted as a function of the chain length. n_c denotes the critical chain length of the detaching chains. (b) The critical chain length n_c and (c) normalized nominal stress plotted as functions of increasing stretch λ and varied bonding strength f_{str}. (d) The energy dissipation ratio plotted as a function of increasing bonding strength. The inset schematic illustrates the stored elastic energy during the loading and unloading, E_{load} and E_{unload}, respectively. $\Delta E = E_{\text{load}} - E_{\text{unload}}$ denotes the dissipated energy during a loading–unloading cycle.

4. Results

In this section, we will study the stress–stretch behaviors of the nanocomposite hydrogels under uniaxial large deformation with the aid of Eqs. (31), (32) and (41). We will examine the effects of the chain detachment, network alteration, particle concentration, and particle size on the cyclic tensile mechanical behaviors of the nanocomposite hydrogels. Theoretical predictions will be compared with the experimental results of the nanosilica hydrogels.

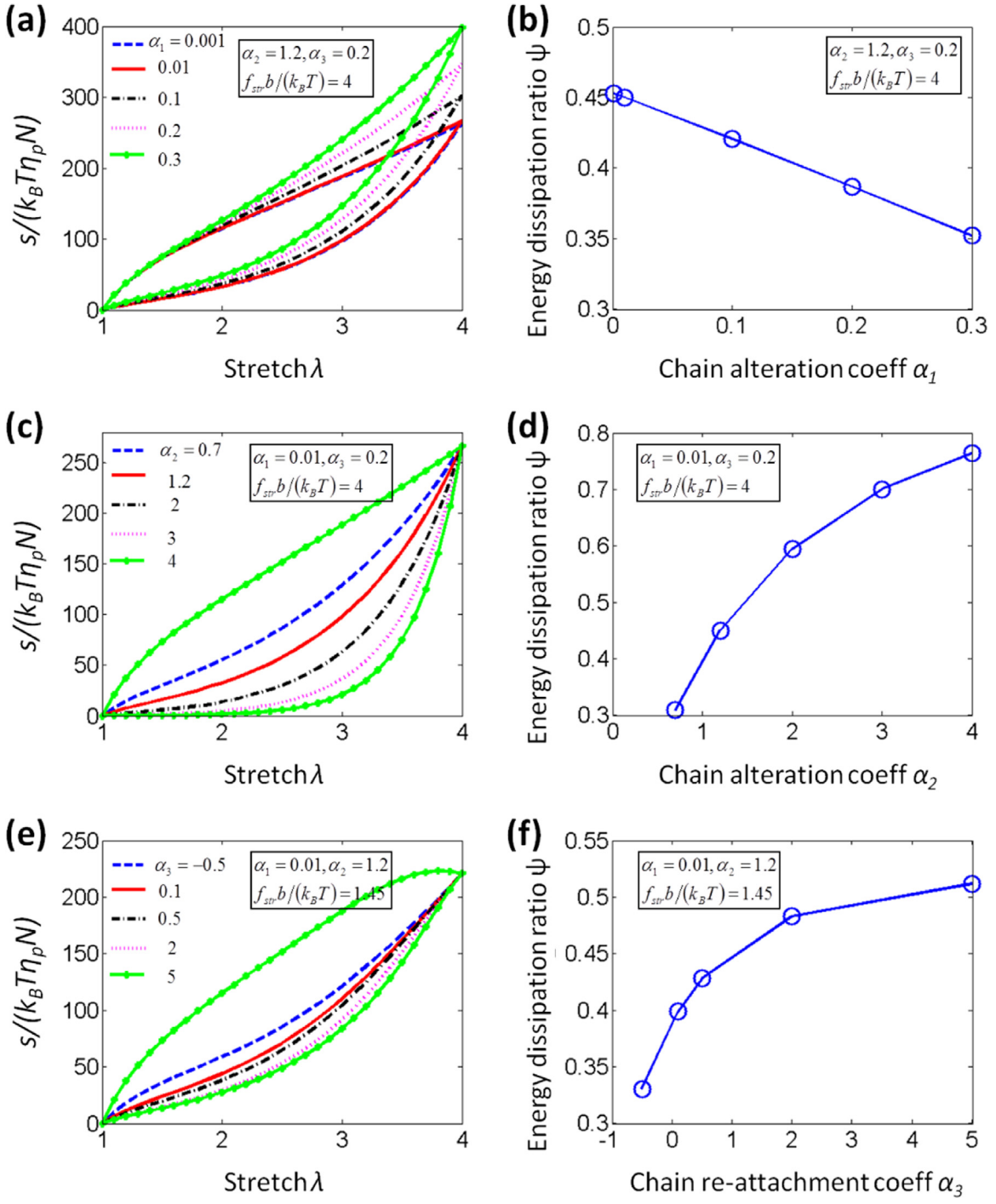

Fig. 8. Effects of chain alternation on the cyclic stress–stretch behaviors of the nanocomposite hydrogels. Nominal stresses plotted as functions of varied stretch for varied (a) chain loading alteration coefficient α_1, (c) chain unloading alteration coefficient α_2 and (d) chain unloading re-attachment coefficient α_3. (b, d and f) The corresponding energy dissipation ratios plotted as functions of chain alternation coefficients α_1, α_2 and α_3, respectively.

4.1. Effect of chain detachment

At the fabricated state, the shortest chains that can attach on the particles have chain length n_1 (Eq. (15)). Under deformation, all chains with shorter length than n_c (gray shadow part) are detached from the particle (Fig. 7a). The critical detachment chain length n_c can be calculated by Eq. (21), where the maximum first invariant of right Cauchy Green tensor is $I_{\max} = (\lambda^2 + \lambda^{-2} + 1)_{\max}$, λ is the uniaxial stretch under a pure-shear stretching condition. As shown in Fig. 7b, the critical detachment chain length n_c monotonically increases with the increasing uniaxial stretch λ. In addition, as the bonding strength f_{str} increases, less chains can be detached from the particles; therefore, the critical detachment chain length n_c decreases with increasing bonding strength (Fig. 7b). For the extreme case, when f_{str} is infinitely large, no chains can be detached from the particles during the deformation.

The detached chains release the free energy of these chains, not only affecting the stress–strain behaviors during the mechanical loading but also inducing energy dissipations through the loading–unloading cycles. To examine the sole effect of chain detachment, we here neglect the network alteration effects in Section 3.2.2.2, namely $\alpha_1 = \alpha_2 = 0$ and $\alpha_3 = \infty$, and plot the cyclic stress–stretch behaviors of the nanocomposite hydrogels for various chain-particle bonding strength in Fig. 7c. With increasing stretch, nominal stress first increases and then become softened due to the chain detachment (Fig. 7c). The larger the bonding strength f_{str}, the stress-softening occurs starting from a larger stretch. If a significant portion of the polymer chains are detached from the particles, the nominal stress may even become decreasing with the increasing stretch (e.g., $f_{str}b/(k_BT) = 1.5$ or 2 in Fig. 7c). This negative stress-softening behavior can lead to the so called necking instability of the hydrogel, which will be discussed in details in Section 5.2 and Fig. 13.

Due to the chain detachment during the mechanical stretching, the stress response of the unloading part is smaller than the loading part, resulting in the Mullins effect (Fig. 7c) (Mullins and Tobin, 1965). Due to the Mullins effect, a portion of elastic energy is dissipated by exhibiting the hysteresis through a loading–unloading cycle. To quantify the energy dissipation, we denote the stored elastic energy of the stretching loading part as E_{load} and that of the unloading part E_{unload} (see inset of Fig. 7d). The hysteresis of the loading–unloading loop dissipates elastic energy $\Delta E = E_{load} - E_{unload}$. Here, we further define the energy dissipation ratio as

$$\psi = \frac{\Delta E}{E_{load}} \tag{42}$$

We plot the dissipated energy ratio as a function of the chain-particle bonding strength. With increasing the bonding strength, the smaller portion of polymer chains can be detached during the mechanical loading; therefore, the loading–unloading hysteresis dissipates smaller portion of elastic energy (Fig. 7d). As the bonding strength increases to large enough (e.g., $f_{str}b/(k_BT) \geq 10$), the energy dissipation ratio decreases to nearly zero as almost no polymer chains are detached (Fig. 7d).

4.2. Effect of network alteration

Besides the effects of the chain detachment, the Mullins effect of the nanocomposite hydrogels can also be attributed to the effects of the network alterations during the mechanical loading–unloading (Fig. 8). First, the chain detachment may increase the number of long chains ($n_c \leq n_i \leq n_m$) (see red chains in Fig. 4ab), indicated by the parameter α_1. According to Eq.

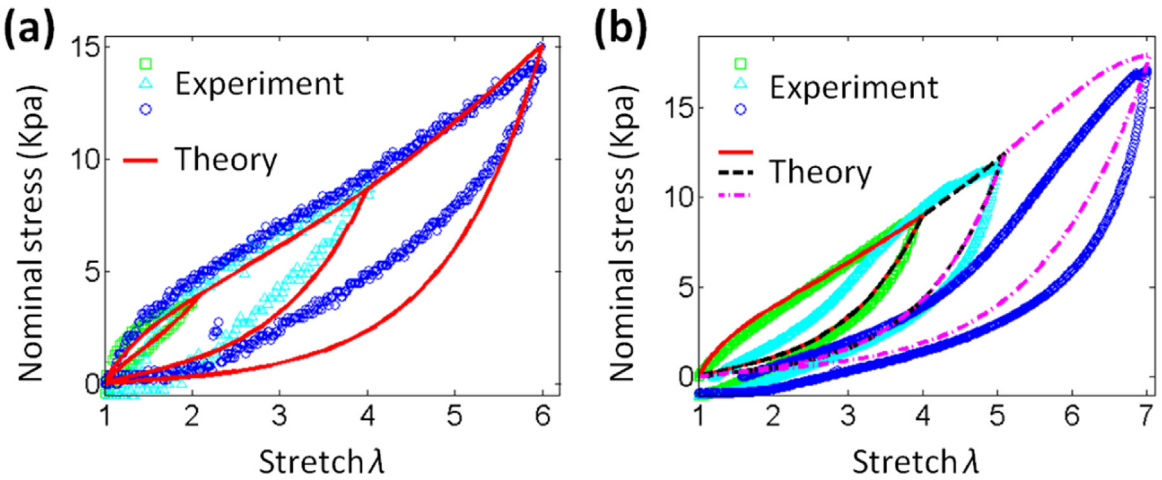

Fig. 9. The comparison of experimentally measured and theoretically predicted stress–stretch behaviors of the nanocomposite hydrogels. (a) Three samples are tested for one cycle but with varied maximum stretches. (b) One sample is tested for three sequential cycles with different maximum stretches. The following parameters are employed to plot the curves: $D/b = 100$,$\kappa = 0.0058$, $\alpha_1 = 0.01$, $\alpha_2 = 1.2$, $\alpha_3 = 0.2$, $f_{str}b/(k_BT) = 4$ and $\eta_p = 8.2 \times 10^{19}\mathrm{m}^{-3}$. (For interpretation of the references to color in this figure, the reader is referred to the web version of this article.)

(25), with increasing α_1 more long chains are generated by the detachment of short chains ($n_1 \le n_i < n_c$), thus leading to higher stress response in the mechanical loading (Fig. 8a). Besides, due to the energy saving by generating long chains, less energy is dissipated by the chain detachment (Fig. 8b).

Second, during the mechanical unloading, the grafting of long chains on the middle particles may transit a number of long chains ($n_{mc} \le n_i \le n_m$) to shorter chains ($n_c \le n_i \le n_{mc}$) (see red and yellow chains in Fig. 4c). The chain grafting effect during the mechanical unloading is parameterized by α_2, and larger α_2 indicates more long chains disappear by the chain grafting (Eq. (26)). By fixing other parameter, increasing α_2 does not affect the stress response in the loading part, but leads to lower stress response in the unloading parts (Fig. 8c). Therefore, the energy dissipation ratio increases with increasing α_2 as shown in Fig. 8d.

Third, in the mechanical unloading, due to chain grafting and chain re-attachment (Fig. 4c), a number of the previously detached short chains ($n_c \le n_i \le n_{mc}$) can become active again. This healing effect of the short chains is indicated by parameter α_3 in Eq. (27). With decreasing α_3, more active short chains ($n_c \le n_i \le n_{mc}$) are generated during the mechanical loading, thus generating higher stress response in the unloading parts in Fig. 8e. It is noted that when α_3 is negative, the number of active short chains can be higher than the original one at the fabricated state, because the grafting of long chains during the mechanical unloading may induce significant amount of short chains. Due to healing effect, smaller energy dissipation can thus be expected with decreasing α_3 (Fig. 8f).

4.3. Cyclic tension test

We next compare the theoretical prediction presented in Eq. (31) with the experimentally measured stress–stretch behaviors of the uniaxially cyclic tension tests. In Fig. 9a, three samples (TM-SP2) with the same size (initial gauge dimension: length 4 mm, width 45 mm and thickness 4 mm) are loaded and unloaded with uniaxial pure-shear tension for one cycle with various maximum stretches ($\lambda_{\max}$=2, 4 and 6). The theoretical predictions match the experimental results consistently by setting $\alpha_1 = 0.01$, $\alpha_2 = 1.2$, $\alpha_3 = 0.2$ and $f_{str}b/(k_BT) = 4$ (Fig. 9a). By using the same set of parameters, the theoretical predictions can also agree relatively well with the experimentally measure stress–stretch behaviors of a sequential cyclic tensions of a TM-SP2 hydrogel sample (Fig. 9b). It is noted that due to the Mullins effect the stress–stretch behaviors of the non-virgin loading part should follow the unloading route of the previous cycle (see the intersection between the solid red line and dashed black line, or between the dashed black line and the dotted pink line) (Fig. 9b). The experimentally observed behaviors may offset in the intersection parts but still qualitatively follow the theoretical predictions (Fig. 9b). The discrepancy may come from the viscoelasticity of the hydrogel that we have not considered in the current model.

4.4. Effect of particle concentration

The stress–stretch behaviors can be significantly affected by the particle concentration in the nanocomposite hydrogels. First, the nominal stress is a linear relationship with the particle concentration η_p (Eqs. (31) and (32)). Second, the particle concentration η_p is directly related to the distance of the particle through Eq. (4), thus affecting the chain length distribution

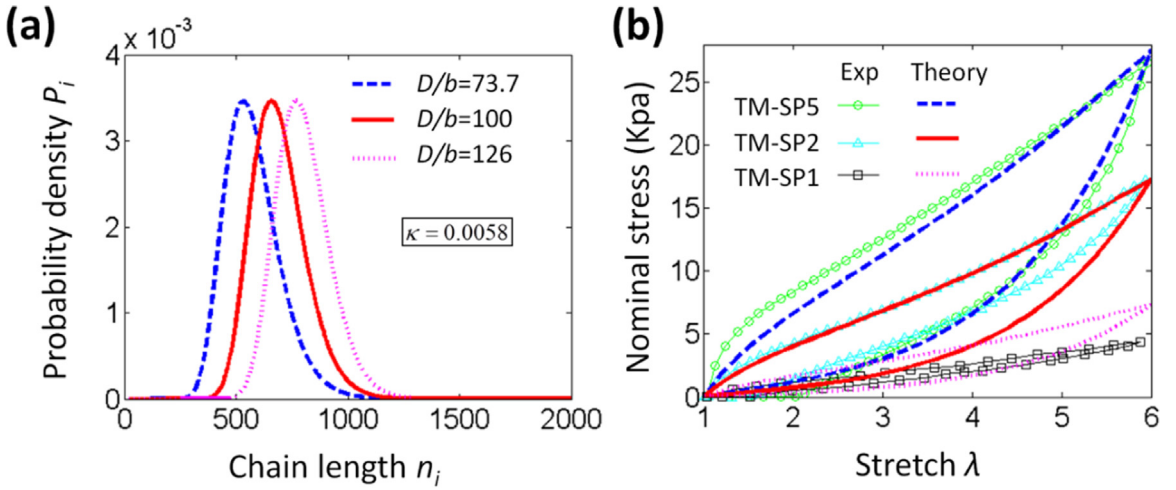

Fig. 10. Effects of particle concentrations on the stress–stretch behaviors of the nanocomposite hydrogels. (a) Chain probability density plotted as functions of the chain length for varied particle pair distance. (b) Experimentally measured (Carlsson et al., 2010) and theoretically predicted stress–stretch behaviors of the nanocomposite hydrogels for varied particle concentrations. "SP5", "SP2" and "SP1" denotes particle concentration $\eta_p = 20.5 \times 10^{19}\text{m}^{-3}$, $\eta_p = 8.2 \times 10^{19}\text{m}^{-3}$ and $\eta_p = 4.2 \times 10^{19}\text{m}^{-3}$, respectively (Table 1). The following parameters are employed to plot theoretical curves in (b): $\alpha_1 = 0.01$, $\alpha_2 = 0.8$, $\alpha_3 = 0.2$, $f_{str}b/(k_BT) = 4$.

through Eqs. (40) and (41). For example, the particle distances of the nanocomposite hydrogels with particle concentration $4.1 \times 10^{19}\mathrm{m}^{-3}$ (TM-SP1), $8.2 \times 10^{19}\mathrm{m}^{-3}$ (TM-SP2) and $20.5 \times 10^{19}\mathrm{m}^{-3}$ (TM-SP5) (see Table 1) can be respectively calculated as $D/b = 73.7$, 100 and 126, thus showing varied chain length distribution in Fig. 10a. Carlsson et al. (2010), measured the stress–stretch behaviors of nanocomposite hydrogels with varied particle concentrations, shown in Fig. 10b. The uniaxial tension tests are performed by setting the initial gauge length is much larger than the width; therefore, the stretch state should be $\lambda_1 = \lambda$ and $\lambda_2 = \lambda_3 = \lambda^{-1/2}$. The nominal stress–stretch relationship can be written as Eq. (32), which is plotted for nanocomposite hydrogels with various particle concentrations in Fig. 10b. The theoretical predictions for high particle concentrations (SP5 and SP2) quantitatively agree with the experimental results (Carlsson et al., 2010), while the prediction for the low concentration case (SP1) only shows qualitative agreement. The discrepancy is probably because that the hydrogel with lower particle concentration is softer and thus may show more evident viscoelastic effect that the current model does not consider.

4.5. Effect of particle size

The particle size can also affect the stress–stretch behaviors of the nanocomposite hydrogels. The particle size may affect two physical parameters: the particle activity κ in Eq. (36) and the attaching chain number N between the particle pair in Eq. (6). For the particles we consider in the current paper, we assume the particles are fabricated with the same method, and we deposit the same amount of redox initiators (See Table 1); therefore, we assume the number of the active sites N_{site} for attaching polymer chains is proportional to the surface area of the particle ($\sim 4\pi r^2$). Therefore, the particle activity κ in Eq. (36) is the same for the particles considered in the current paper. In turn, the number of active sites on a particle can be expressed as

$$N_{site} = \frac{4r^2\kappa}{b^2} \tag{43}$$

We further assume each active site has been bonded to a polymer chain. Since the active sites on one particle should be averagely connected to polymer chains for 4 particle pairs (Figs. 2 and 3), the attaching chain number (Eq. (6)) between as particle pair can thus be approximated as

$$N \sim \frac{N_{site}}{4} = \frac{r^2\kappa}{b^2} \tag{44}$$

which shows that N is proportional to the square of the particle size r.

Here, we examine the effects of particle sizes by using three types of particles with size $r = 7.5$ nm (TM-SP2), 4.5 nm (HS-SP2) and 2.5 nm (SM-SP2), respectively (see Table 1) (Rose et al., 2014). To isolate the effect of the particle sizes, we set the particle concentration in the hydrogel to be the same, thus the chain length distribution the same for three samples with varied particle sizes (Fig. 11a). The predicted stress–stretch behaviors by using Eqs. (44) and (31) quantitatively agree with the measured experimental results for various particle sizes (Fig. 11b). Existing discrepancy comes from the unconsidered viscoelastic effects mentioned in Sections 4.3 and 4.4, as well as the assumption that the active site number is proportional

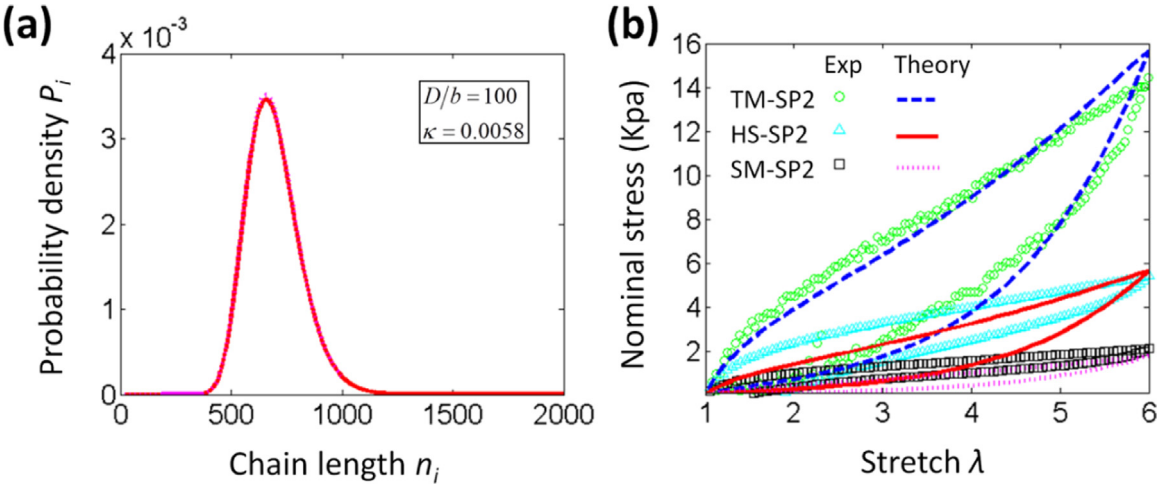

Fig. 11. Effects of particle sizes on the stress–stretch behaviors of the nanocomposite hydrogels. (a) Chain probability density plotted as functions of the chain length for varied particle pair distance. (b) Experimentally measured and theoretically predicted stress–stretch behaviors of the nanocomposite hydrogels for varied particle sizes. "TM", "HS" and "SM" denotes nanoparticles with radius r=7.5 nm, r=4.5 nm and r=2.5 nm, respectively (Table 1). The following parameters are employed to plot theoretical curves in (b): $\alpha_1 = 0.01$, $\alpha_2 = 0.8$, $\alpha_3 = 0.2$, $f_{str}b/(k_BT) = 4$, $N_{site}=108$ (r=7.5 nm), $N_{site}=39$ (r=4.5 nm) and $N_{site}=12$ (r=2.5 nm).

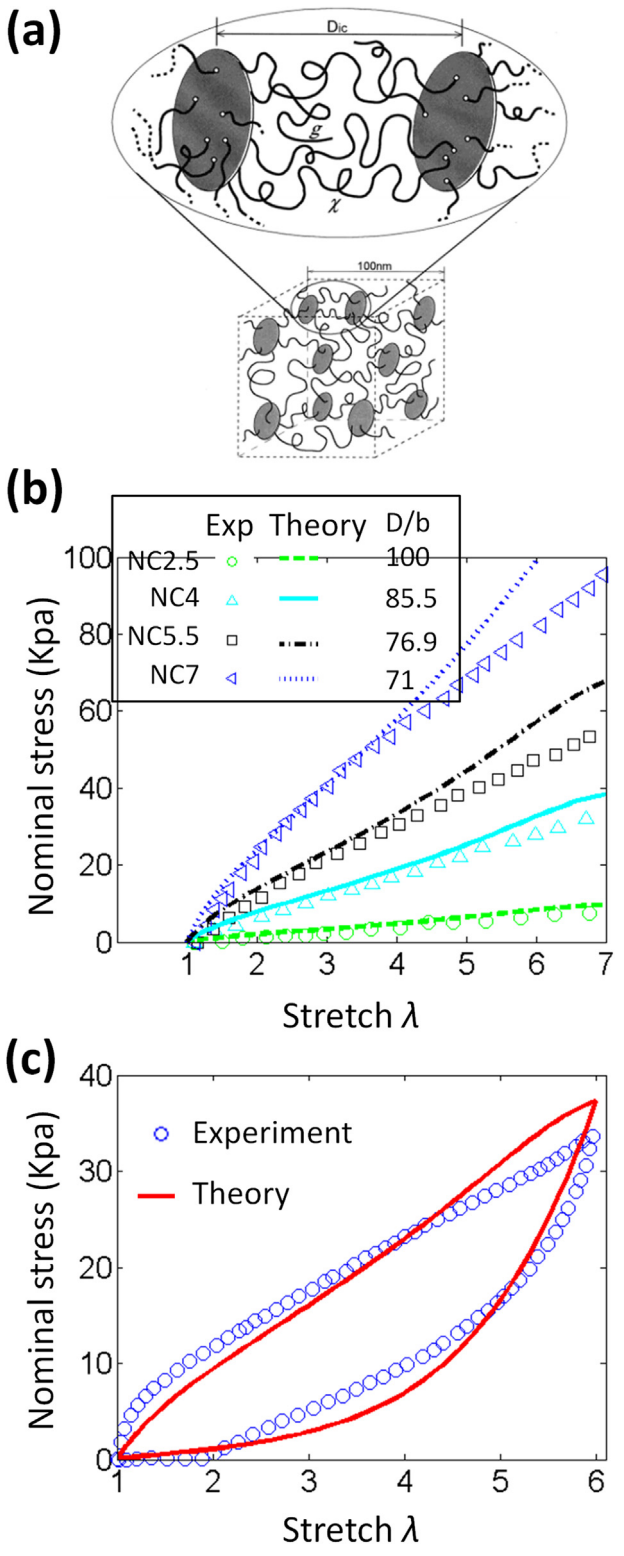

Fig. 12. (a) A schematic to show the molecular structure of the nanoclay hydrogel. Figure from reference (Haraguchi et al., 2002). The experimentally measured and theoretically predicted stress–stretch behaviors of (b) uniaxial stretching nanoclay hydrogels with varied nanoclay concentrations and (c) a nanoclay hydrogel under a cyclic loading–unloading. The experimental data in (b) and (c) are reproduced from Haraguchi et al. (2002) and Klein et al. (2015), respectively. The following parameters are employed to plot theoretical curves in (b) and (c): $\kappa = 0.0058$, $\alpha_1 = 0.01$, $\alpha_2 = 1.2$, $\alpha_3 = 0.2$, $f_{str}b/(k_BT) = 4$and $N_{site} = 108$.

to the surface area. It is highly possible that the smaller particles have stronger capability to absorb more redox initiators per unit surface area, which, however, is not considered in this section.

5. Applications of the theory

Besides the silica nanoparticles used in Sections 2 and 4, a number of nanoparticles have been used to crosslink polymer chains into nanocomposite hydrogel networks, including nanoclay, silsesquioxane, titania, graphene oxcide and carbon nanotubes (Carlsson et al., 2010; Haraguchi, 2007, 2011a,b; Haraguchi et al., 2003, 2007, 2002, 2011; Haraguchi and Li, 2006, 2005; Haraguchi and Song, 2007; Haraguchi and Takehisa, 2002; Huang et al., 2007; Ren et al., 2011; Wang et al., 2010). The theory constructed in the current paper can be useful not only for the nanosilica hydrogels, but also probably for hydrogels with other nanoparticle crosslinkers. In this section, we will apply the theory to predict the mechanical behaviors of the nanoclay hydrogels that use exfoliated nanoclay particles to crosslink polymer chains N,N-Dimethylacrylamide or N-Isopropylacrylamide (Fig. 12a) (Haraguchi, 2007, 2011b; Haraguchi and Takehisa, 2002).

5.1. Stress–strain behaviors of nanoclay hydrogels

To synthesize the nanoclay hydrogels, Haraguchi, et al. used Laponite XLG nanoclays that are in disk shape with dimension around 30 nm in diameter and 1 nm in thickness (Fig. 12a) (Haraguchi, 2007, 2011b; Haraguchi and Takehisa, 2002). The active sites on the nanoclay surfaces form physical bonds with the polymer chains and thus crosslink the polymer chains into networks. Haraguchi et al. (2003) measured the stress–stretch behaviors of the nanoclay hydrogels with various nanoclay concentrations as reproduced in Fig.12b. The stress responses increase with increasing clay concentrations.

To model the nanoclay hydrogels here, we approximate the disk-shaped nanoclays (Fig. 12a) as spherical particles as

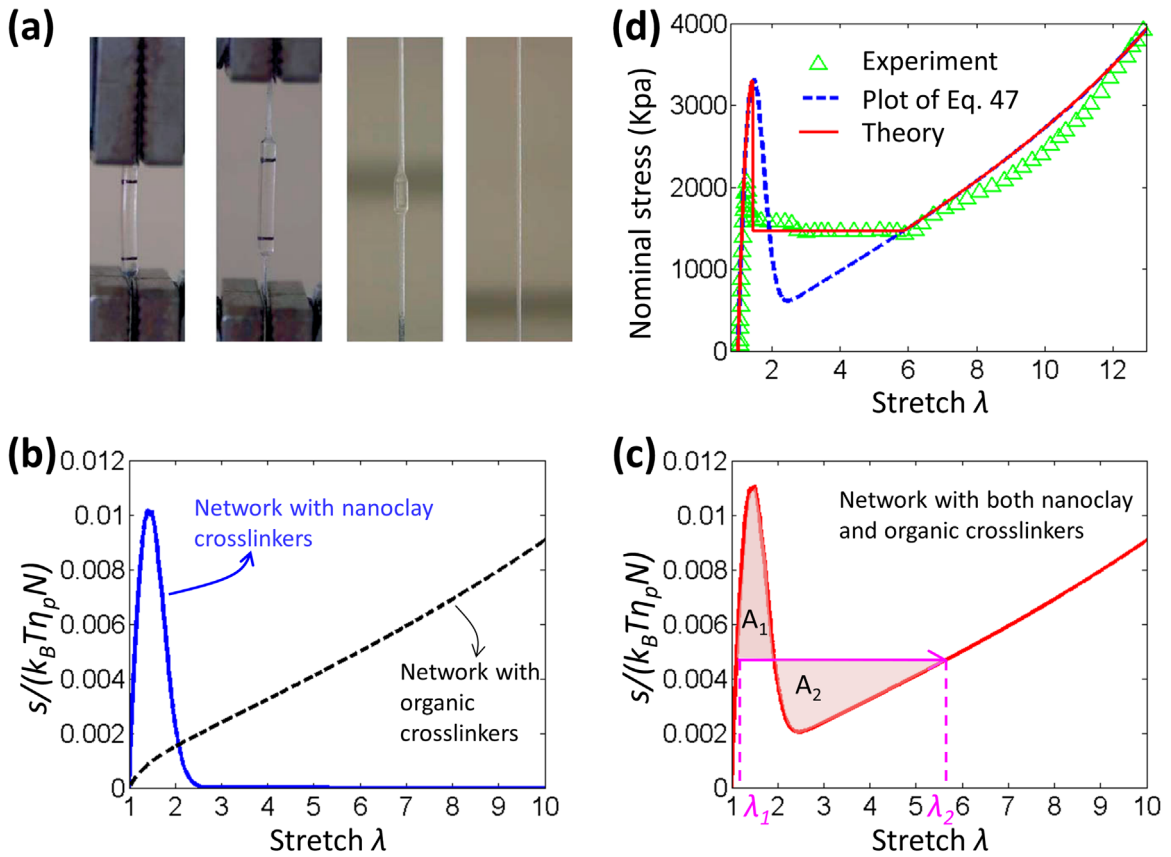

Fig. 13. (a) Experimentally observed necking instability of the composite hydrogel with both nanoclay and organic crosslinkers (Haraguchi et al., 2006). The stress–stretch behaviors of (b) the networks with nanoclay crosslinkers and organic crosslinkers, respectively, and (c) the interpenetrating network with both crosslinkers. (d) The theoretically predicted and experimentally measured stress–stretch behaviors of the composite hydrogel with both crosslinkers through necking instability. The following parameters are employed to plot theoretical curves in (b–d): $D/b = 100$, $\kappa = 0.00195$, $\alpha_1 = 0.01$, $\alpha_2 = 1.2$, $\alpha_3 = 0.2$ $f_{str}\, b/(k_B T) = 1.24$, $N_{site} = 108$, and $n_{org} = 200$.

shown in Figs. 2 and 3. To ensure the same number of active sites on nanoparticle surfaces, we set the surface area of the spherical particles the same as that of the nanoclays by assuming the active site densities on both nanoparticles are the same. Therefore, the radius of the spherical nanoparticles is calculated as 7.5 nm. Following the similar procedure in Section 4.4, we estimate the particle distance D, and use Eq. (32) to plot out the stress–stretch behaviors of the nanoclay hydrogels for various nanoclay concentrations in Fig. 12b. The theoretical predictions match consistently with the experimental results (Haraguchi et al., 2003). In addition, by following Eq. (32), the cyclic stress behaviors can also be predicted, in good agreement with the experimentally measured results (Klein et al., 2015).

5.2. Necking instability of nanocomposite hydrogels with both nanoclay and organic crosslinkers

Haraguchi et al. (2006) incorporated both nanoclay crosslinkers and organic crosslinkers within the nanocomposite hydrogels and found out the hydrogels exhibited necking instability under the uniaxial tension (reproduced in Fig. 13a). We can understand the necking instability of the composite hydrogel as follows. We consider that the hydrogel consists of two interpenetrating networks: the nanoclay crosslinked network and organically crosslinked network. The free energy density of stretching the composite hydrogel can thus be written as

$$W_{com} = W_{nano} + W_{org} \tag{45}$$

where the free energy density of the nanoclay network $W_{nano} = 4\eta_p \sum_{i=c}^{m} [\omega_i(n_{ia}, \Lambda_i)N_{ia}]$ comes from Eq. (28) and W_{chem} is the free energy density of stretching the organically crosslinked network. Here, we model the organically crosslinked network by following the eight-chain model (Arruda and Boyce, 1993) with the free energy density expressed as

$$W_{org} = N_{org} n_{org} k_B T \left[\frac{\beta_{org}}{\tanh \beta_{org}} + \ln\left(\frac{\beta_{org}}{\sinh \beta_{org}} \right) \right] \tag{46}$$

where n_{org} is the average chain length, N_{org} is the chain number per unit volume of the network, $\beta_{org} = L^{-1}(\Lambda_{org}/\sqrt{n_{org}})$, $\Lambda_{org} = \sqrt{I_1/3}$ is the chain stretch of the organically crosslinked polymer chain and I_1 is the first invariant of the right Cauchy Green tensor. Under pure-shear uniaxial stretch with $\lambda_1 = \lambda$ and $\lambda_2 = \lambda_3 = \lambda^{-1/2}$, the nominal stress of the composite hydrogel consists two parts, namely

$$s_{com} = s_{nano} + s_{org} \tag{47}$$

where the nominal stress of the nanoclay-crosslinked network s_{nano} can be written as Eq. (32), and the nominal stress of the chemically crosslinked network can be calculated from Eq. (46) as,

$$s_{org} = \frac{N_{org}\sqrt{n_{org}} k_B T \beta_{org}}{3\Lambda_{org}} \left(\lambda - \lambda^{-2} \right) \tag{48}$$

We hypothesize that necking instability of the nanocomposite hydrogels with two interpenetrating networks is due to breaking of the nanoclay networks with short polymer chains and backing-up of the organic networks with long polymer chains. During the stretching, the nanoclay-assisted polymer chains are first stretched out and detached from the nanoclays due to short chain length or small polymer-particle bonding strength; therefore, the stress response of the nanoclay network first quickly goes up, and then goes down due to the chain detachment (Eq. (32), Fig. 13b). However, the stress response of the organically crosslinked polymer network, consisting of long polymer chains, slowly increases with the increasing stretch (Eq. (48)). At low stretch λ, the nanoclay network dominates over the organically crosslinked network; while at high stretch λ, most of the nanoclay-bonded chains are detached and the organically crosslinked network prevails. Overall, the nominal stress response of the composite hydrogel, predicted by Eq. (48), goes up, down and up again as shown in Fig. 13c. According to Maxwell rule (Abeyaratne and Knowles, 2006; Ericksen, 1998; Gurtin, 2012), two states, thick region with stretch λ_1 and thin region with stretch λ_2, coexist in the hydrogel when the area of the two shaded regions A_1 and A_2 have the same area in Fig. 3c. Experimentally (images in Fig. 3a and data in Fig. 3d) (Haraguchi et al., 2006), the nominal stress first increases to the peak point and the necking of the bar sets in with the stress quickly relaxed to the stress level for the coexistence state. Upon further stretching, the minimal stress maintains while the thin necking region propagates with the consumption of the thick region of the bar. Once the hydrogel bar totally thins down, the nominal stress increases again. As shown in Fig. 13d, our theory can consistently predict the stress–stretch behaviors of the stretching bar through the necking instability.

6. Conclusive remarks

In Summary, we present a constitutive model for nanocomposite hydrogels with only nanoparticle crosslinkers. We consider the nanoparticles form physical bonds with the polymer chains and crosslink the polymer chains into body-centered microarchitectures. Between two particles, a number of polymer chains with inhomogeneous lengths are attached on the particles. Once deformed, the polymer chains with inhomogeneous chain lengths are sequentially detached from the

particles. We further consider the polymer chains can evolve with chain alteration and re-attachment. We show that our constitutive model can well predict the experimentally observed Mullins effects of the nanocomposite hydrogels under multiple loading–unloadings. By using the model, we can also capture the effects of the particle concentrations and size on the cyclic stress–stretch behaviors of nanocomposite hydrogels, in good agreement with experimental results of model nanosilica hydrogels. In addition to nanosilica hydrogels, we further show that the constitutive theory is also applicable to revealing the mechanical behaviors of the hydrogels with only nanoclay crosslinkers, and the necking instability of composite hydrogels with both nanoclay and organic crosslinkers.

We note that in this model we assume that any polymer chains with the same length, including initially-attached and reattached chains, have the same stretching free energy at a certain macroscopic strain invariant I_1 (illustrated by Eq. (28)). This assumption is only valid when the chain relaxation time scale is much larger than the loading–unloading time scale. When the chain relaxation time scale is comparable or smaller than the loading–unloading time scale, the reattached polymer chains should not be treated with the same stretching free energy as the initially attached chains. Under these conditions, more careful assessment on the kinetics of the chain detaching-reattaching is indispensably needed (Green and Tobolsky, 1946; Hui and Long, 2012; Long et al., 2014).

The constitutive model may provide insight to designing tough hydrogels with high stretchability. For example, Figs. 7 and 8 reveal that adequate modulating the chain-polymer interactions (e.g., particle-chain bonding strength, chain alteration, chain grafting and rehealing) may offer a route to design hydrogels with high energy dissipation during the mechanical-loading unloading while maintaining high stretchability, thus achieving high toughness. As another example, the theory presented in Section 5.2 implies that it is may be a good strategy to synthesize tough nanocomposite hydrogels by designing interpenetrating networks with nanoclay networks with short chains and covalently crosslinked networks with long chains. This strategy echoes the idea of double-network hydrogels with ionic networks and covalent networks (Gong et al., 2003; Long et al., 2014; Sun et al., 2012). Moreover, the constitutive model may further facilitate the design of novel polymer-particle interactions and polymer chain dynamics for diverse applications in material science, chemical synthesis and biology (Appel et al., 2015; Hui and Long, 2012; Long et al., 2013; Rose et al., 2014; Wang et al., 2010; Williams et al., 2015).

Acknowledgment

The work is supported by start-up fund from the University of Southern California.

References

Abeyaratne, R., Knowles, J.K., 2006. In: Evolution of Phase Transitions: a Continuum TheoryCambridge University Press, Cambridge.
An, Y., Solis, F.J., Jiang, H., 2010. A thermodynamic model of physical gels. J. Mech. Phys. Solids 58, 2083–2099.
Appel, E.A., Tibbitt, M.W., Webber, M.J., Mattix, B.A., Veiseh, O., Langer, R., 2015. Self-assembled hydrogels utilizing polymer–nanoparticle interactions. Nat. Commun. 6, 6295.
Arruda, E.M., Boyce, M.C., 1993. A three-dimensional constitutive model for the large stretch behavior of rubber elastic materials. J. Mech. Phys. Solids 41, 389–412.
Blanchard, A., Parkinson, D., 1952. Breakage of carbon-rubber networks by applied stress. Ind. Eng. Chem. 44, 799–812.
Bueche, F., 1960. Molecular basis for the Mullins effect. J. Appl. Polym. Sci. 4, 107–114.
Carlsson, L., Rose, S., Hourdet, D., Marcellan, A., 2010. Nano-hybrid self-crosslinked PDMA/silica hydrogels. Soft Matter 6, 3619–3631.
Chagnon, G., Verron, E., Marckmann, G., Gornet, L., 2006. Development of new constitutive equations for the Mullins effect in rubber using the network alteration theory. Int. J. Solids Struct. 43, 6817–6831.
Dargazany, R., Itskov, M., 2009. A network evolution model for the anisotropic Mullins effect in carbon black filled rubbers. Int. J. Solids Struct. 46, 2967–2977.
de Gennes, P.G., 1971. Reptation of a polymer chain in the presence of fixed obstacles. J. Chem. Phys. 55, 572–579.
Diani, J., Fayolle, B., Gilormini, P., 2009. A review on the Mullins effect. Eur. Polym. J. 45, 601–612.
Dorfmann, A., Ogden, R., 2003. A pseudo-elastic model for loading, partial unloading and reloading of particle-reinforced rubber. Int. J. Solids Struct. 40, 2699–2714.
Ericksen, J.L., 1998. Introduction to the Thermodynamics of Solids. Springer Science & Business Media, Berlin.
Erman, B., Mark, J.E., 1997. In: Structures and Properties of Rubberlike NetworksOxford University Press, Oxford.
Flory, P.J., 1953. In: Principles of Polymer ChemistryCornell University Press, Ithaca.
Flory, P.J., Rehner Jr, J., 1943. Statistical mechanics of cross-linked polymer networks II. Swelling. J. Chem. Phys. 11, 521–526.
Gong, J.P., Katsuyama, Y., Kurokawa, T., Osada, Y., 2003. Double-network hydrogels with extremely high mechanical strength. Adv. Mater. 15, 1155–1158.
Govindjee, S., Simo, J., 1991. A micro-mechanically based continuum damage model for carbon black-filled rubbers incorporating Mullins' effect. J. Mech. Phys. Solids 39, 87–112.
Green, M.S., Tobolsky, A.V., 1946. A new approach to the theory of relaxing polymeric media. J. Chem. Phys. 14, 80–92.
Gurtin, M., 2012. In: Phase Transformations and Material Instabilities in SolidsElsevier, Philadelphia.
Haraguchi, K., 2007. Nanocomposite hydrogels. Curr. Opin. Solid State Mater. Sci. 11, 47–54.
Haraguchi, K., 2011a. Stimuli-responsive nanocomposite gels. Colloid Polym. Sci. 289, 455–473.
Haraguchi, K., 2011b. Synthesis and properties of soft nanocomposite materials with novel organic/inorganic network structures. Polym. J. 43, 223–241.
Haraguchi, K., Ebato, M., Takehisa, T., 2006. Polymer–clay nanocomposites exhibiting abnormal necking phenomena accompanied by extremely large reversible elongations and excellent transparency. Adv. Mater. 18, 2250–2254.
Haraguchi, K., Farnworth, R., Ohbayashi, A., Takehisa, T., 2003. Compositional effects on mechanical properties of nanocomposite hydrogels composed of poly (N, N-dimethylacrylamide) and clay. Macromolecules 36, 5732–5741.
Haraguchi, K., Li, H.-J., 2006. Mechanical properties and structure of polymer–clay nanocomposite gels with high clay content. Macromolecules 39, 1898–1905.

Haraguchi, K., Li, H.-J., Song, L., Murata, K., 2007. Tunable optical and swelling/deswelling properties associated with control of the coil-to-globule transition of poly (N-isopropylacrylamide) in polymer–clay nanocomposite gels. Macromolecules 40, 6973–6980.
Haraguchi, K., Li, H.J., 2005. Control of the coil-to-globule transition and ultrahigh mechanical properties of PNIPA in nanocomposite hydrogels. Angew. Chem. Int. Ed. 44, 6500–6504.
Haraguchi, K., Song, L., 2007. Microstructures formed in co-cross-linked networks and their relationships to the optical and mechanical properties of PNIPA/clay nanocomposite gels. Macromolecules 40, 5526–5536.
Haraguchi, K., Takehisa, T., 2002. Nanocomposite hydrogels: a unique organic-inorganic network structure with extraordinary mechanical, optical, and swelling/de-swelling properties. Adv. Mater. 14, 1120–1124.
Haraguchi, K., Takehisa, T., Fan, S., 2002. Effects of clay content on the properties of nanocomposite hydrogels composed of poly (N-isopropylacrylamide) and clay. Macromolecules 35, 10162–10171.
Haraguchi, K., Uyama, K., Tanimoto, H., 2011. Self-healing in nanocomposite hydrogels. Macromol. Rapid Commun. 32, 1253–1258.
Hong, W., Zhao, X., Zhou, J., Suo, Z., 2008. A theory of coupled diffusion and large deformation in polymeric gels. J. Mech. Phys. Solids 56, 1779–1793.
Huang, T., Xu, H., Jiao, K., Zhu, L., Brown, H.R., Wang, H., 2007. A novel hydrogel with high mechanical strength: a macromolecular microsphere composite hydrogel. Adv. Mater. 19, 1622–1626.
Hui, C.-Y., Long, R., 2012. A constitutive model for the large deformation of a self-healing gel. Soft Matter 8, 8209–8216.
Iyer, B.V., Yashin, V.V., Balazs, A.C., 2014. Dynamic behavior of dual cross-linked nanoparticle networks under oscillatory shear. J. Phys. 16, 075009.
Iyer, B.V., Yashin, V.V., Kowalewski, T., Matyjaszewski, K., Balazs, A.C., 2013. Strain recovery and self-healing in dual cross-linked nanoparticle networks. Polym. Chem. 4, 4927–4939.
Johnson, M., Beatty, M., 1993. A constitutive equation for the Mullins effect in stress controlled uniaxial extension experiments. Contin. Mechan. Thermodyn. 5, 301–318.
Kamata, H., Akagi, Y., Kayasuga-Kariya, Y., Chung, U.-i, Sakai, T., 2014. “Nonswellable” hydrogel without mechanical hysteresis. Science 343, 873–875.
Keplinger, C., Sun, J.-Y., Foo, C.C., Rothemund, P., Whitesides, G.M., Suo, Z., 2013. Stretchable, transparent, ionic conductors. Science 341, 984–987.
Klein, A., Whitten, P.G., Resch, K., Pinter, G., 2015. Nanocomposite hydrogels: fracture toughness and energy dissipation mechanisms. J. Polym. Sci. Part B: Polym. Phys. 53, 1763–1773.
Kuhn, W., Grün, F., 1942. Beziehungen zwischen elastischen Konstanten und Dehnungsdoppelbrechung hochelastischer Stoffe. Kolloid-Zeitschrift 101, 248–271.
Lion, A., 1996. A constitutive model for carbon black filled rubber: experimental investigations and mathematical representation. Contin. Mech. Thermodyn. 8, 153–169.
Long, R., Mayumi, K., Creton, C., Narita, T., Hui, C.-Y., 2014. Time dependent behavior of a dual cross-link self-healing gel: theory and experiments. Macromolecules 47, 7243–7250.
Long, R., Qi, H.J., Dunn, M.L., 2013. Thermodynamics and mechanics of photochemcially reacting polymers. J. Mech. Phys. Solids 61, 2212–2239.
Marckmann, G., Verron, E., Gornet, L., Chagnon, G., Charrier, P., Fort, P., 2002. A theory of network alteration for the Mullins effect. J. Mech. Phy. Solids 50, 2011–2028.
Miehe, C., 1995. Discontinuous and continuous damage evolution in Ogden-type large-strain elastic materials. Eur. J. Mech. A. Solids 14, 697–720.
Mullins, L., Tobin, N., 1965. Stress softening in rubber vulcanizates. Part I. Use of a strain amplification factor to describe the elastic behavior of filler-reinforced vulcanized rubber. J. Appl. Polym. Sci. 9, 2993–3009.
Na, Y.-H., Kurokawa, T., Katsuyama, Y., Tsukeshiba, H., Gong, J.P., Osada, Y., Okabe, S., Karino, T., Shibayama, M., 2004. Structural characteristics of double network gels with extremely high mechanical strength. Macromolecules 37, 5370–5374.
Na, Y.-H., Tanaka, Y., Kawauchi, Y., Furukawa, H., Sumiyoshi, T., Gong, J.P., Osada, Y., 2006. Necking phenomenon of double-network gels. Macromolecules 39, 4641–4645.
Ogden, R., Roxburgh, D., 1999. A pseudo-elastic model for the Mullins effect in filled rubber. Proc. R. Soc. Lond. A: Math. Phys. Eng. Sci. 455, 2861–2877.
Qi, H., Boyce, M., 2004. Constitutive model for stretch-induced softening of the stress–stretch behavior of elastomeric materials. J. Mech. Phys. Solids 52, 2187–2205.
Ren, H.-y, Zhu, M., Haraguchi, K., 2011. Characteristic swelling–deswelling of polymer/clay nanocomposite gels. Macromolecules 44, 8516–8526.
Rose, S., Prevoteau, A., Elzière, P., Hourdet, D., Marcellan, A., Leibler, L., 2014. Nanoparticle solutions as adhesives for gels and biological tissues. Nature 505, 382–385.
Rubinstein, M., Colby, R., 2003. In: Polymer PhysicsOxford University Press, Oxford.
Sun, J.-Y., Zhao, X., Illeperuma, W.R., Chaudhuri, O., Oh, K.H., Mooney, D.J., Vlassak, J.J., Suo, Z., 2012. Highly stretchable and tough hydrogels. Nature 489, 133–136.
Sun, T.L., Kurokawa, T., Kuroda, S., Ihsan, A.B., Akasaki, T., Sato, K., Haque, M.A., Nakajima, T., Gong, J.P., 2013. Physical hydrogels composed of polyampholytes demonstrate high toughness and viscoelasticity. Nat. Mater. 12, 932–937.
Tanaka, Y., Gong, J.P., Osada, Y., 2005. Novel hydrogels with excellent mechanical performance. Progr. Polym. Sci. 30, 1–9.
Treloar, L.R.G., 1975. In: The Physics of Rubber ElasticityOxford University Press, Oxford.
Wang, Q., Gossweiler, G.R., Craig, S.L., Zhao, X., 2015. Mechanics of mechanochemically responsive Elastomers. J. Mech. Phys. Solids 82, 320–344.
Wang, Q., Mynar, J.L., Yoshida, M., Lee, E., Lee, M., Okuro, K., Kinbara, K., Aida, T., 2010. High-water-content mouldable hydrogels by mixing clay and a dendritic molecular binder. Nature 463, 339–343.
Wang, X., Hong, W., 2011. Pseudo-elasticity of a double network gel. Soft Matter 7, 8576–8581.
Williams, G.A., Ishige, R., Cromwell, O.R., Chung, J., Takahara, A., Guan, Z., 2015. Mechanically robust and self-healable superlattice nanocomposites by self-assembly of single-component “sticky” polymer-grafted nanoparticles. Adv. Mater. 27, 3934–3941.
Zhao, X., 2012. A theory for large deformation and damage of interpenetrating polymer networks. J. Mech. Phys. Solids 60, 319–332.
Zhao, X., 2014. Multi-scale multi-mechanism design of tough hydrogels: building dissipation into stretchy networks. Soft Matter 10, 672–687.